Cell Reports
Physical Science

CellPress
OPEN ACCESS

Article

Heterogeneous singlet fission in a covalently linked pentacene dimer

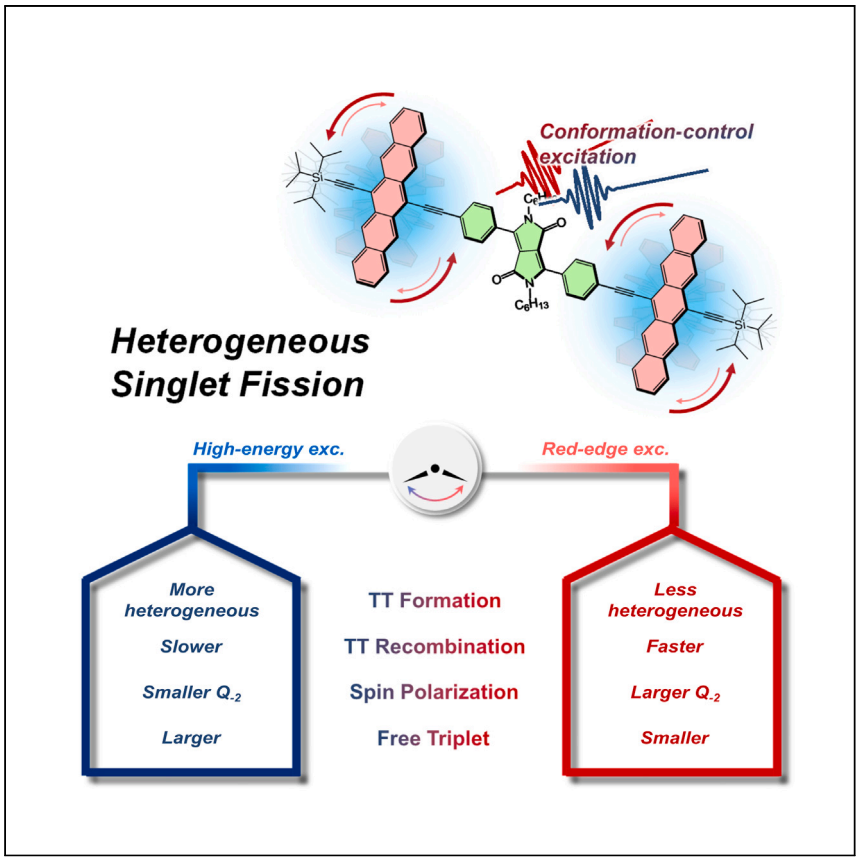

Molecular dimers are frequently viewed as static systems but actually exhibit important dynamic conformational changes in the condensed phase. Here, by excitation-energy-dependent time-resolved optical and spin-resonance experiments, Kim and Panjwani et al. demonstrate heterogeneous singlet fission dynamics in a pentacene dimer, resulting from the interplay of static and dynamic structural inhomogeneity.

Woojae Kim, Naitik A. Panjwani, K.C. Krishnapriya, ..., Robert Bittl, Satish Patil, Andrew J. Musser

naitik.panjwani@fu-berlin.de (N.A.P.)
spatil@iisc.ac.in (S.P.)
ajm557@cornell.edu (A.J.M.)

Highlights

A pentacene dimer shows heterogeneous singlet fission

Static and dynamic structural heterogeneity strongly influence triplet-pair dynamics

Varying excitation energy is necessary to understand the heterogeneity effect

Distribution of sub-ensembles should be considered even in a simple dimer

Kim et al., Cell Reports Physical Science 5, 102045
July 17, 2024
https://doi.org/10.1016/j.xcrp.2024.102045

Cell Reports
Physical Science

CellPress
OPEN ACCESS

Article

Heterogeneous singlet fission in a covalently linked pentacene dimer

Woojae Kim,[1,5,6] Naitik A. Panjwani,[2,6,*] K.C. Krishnapriya,[3] Kanad Majumder,[3] Jyotishman Dasgupta,[4] Robert Bittl,[2] Satish Patil,[3,*] and Andrew J. Musser[1,7,*]

SUMMARY

Molecular dimers are generally regarded as essential tools for probing structure-property relationships in condensed-phase systems, revealing complexities where structural tuning is challenging. Traditionally treated as "static," with properties defined by their optimized geometry, we argue that dimers are "dynamic," exhibiting considerable conformational heterogeneity over time, which significantly influences interchromophore coupling strengths. Illustrating this, we explore the singlet fission dynamics of a pentacene dimer linked by phenyl-diketopyrrolopyrrole and acetylene bridges. The unrestricted rotations yield a myriad of rotational conformers, each altering the singlet fission processes, evident through excitation-energy-dependent transient absorption and electron paramagnetic resonance spectroscopy. This necessitates considering not only broad distribution of rate constants but also multidimensional potential-energy surfaces with multiple sub-ensembles, leading to "heterogeneous singlet fission." Consequently, these findings challenge the prevailing static approach to molecular dimer photophysics, suggesting that individual steps in excited-state relaxation pathways cannot be delineated by unique rate constants and yields.

INTRODUCTION

The bulk of optoelectronic processes in molecular systems are intermolecular in nature.[1–3] Phenomena such as energy transfer, charge transport, electron-hole separation, excimer formation, exciton multiplication through singlet fission (SF), and triplet-triplet annihilation upconversion are chiefly studied in solid films,[4–10] which are most relevant for eventual applications. However, it remains an outstanding challenge to rationally control the intermolecular interactions that drive these processes in the solid state. Moreover, the substantial disorder present in typical thin films can result in a wide distribution of underlying photophysical rates, which can exhibit profound differences from the corresponding single crystals that can be difficult to understand.[11–13] One widespread way to address this challenge is to use tailored molecular dimers as model systems for complex solid-phase photophysics.[14–16] Dimers are significant not just because they represent the minimal unit required for a specific photoinduced reaction but also due to the flexibility with which chromophores and their connections can be manipulated synthetically. Experiments with molecular dimers allow for precise control over the surrounding environment, offering unique mechanistic insights that are challenging to obtain with solid thin films. Moreover, molecular dimers possess more easily defined structures than chromophores in thin films, enabling control of through-bond and through-space couplings.[17–19] This allows the formulation of design principles rooted in a

[1]Department of Chemistry and Chemical Biology, Cornell University, Ithaca, NY 14850, USA

[2]Berlin Joint EPR Lab, Fachbereich Physik, Freie Universität Berlin, 14195 Berlin, Germany

[3]Solid State and Structural Chemistry Unit, Indian Institute of Science, Bangalore 560012, India

[4]Department of Chemical Sciences, Tata Institute of Fundamental Research, Mumbai 400005, India

[5]Department of Chemistry, Yonsei University, Seoul 03722, Republic of Korea

[6]These authors contributed equally

[7]Lead contact

*Correspondence:
naitik.panjwani@fu-berlin.de (N.A.P.),
spatil@iisc.ac.in (S.P.),
ajm557@cornell.edu (A.J.M.)

https://doi.org/10.1016/j.xcrp.2024.102045

comprehensive library of structure-property relationships behind excited-state dynamics from ultrafast charge separation and SF to the slow evolution of entangled spin states.[20–25] However, some caution is warranted with this approach. Although they often exhibit narrower linewidths and thus less disorder than thin films, such dimers can exhibit a broad array of interchromophore orientations, depending on the chemical nature and position of the linkers.[26–29] This intramolecular conformational heterogeneity is not often treated as an important contributor to either the dynamics or the balance of product states. Instead, common practice is to consider only a single ensemble, assuming quasi-static structures based on the equilibrium geometries of the relevant electronic states, for the interpretation of the photophysics in dimers.

This kind of interpretation is widespread in the study of SF, in which a photoexcited singlet exciton (S_1) generates two triplet excitons ($T_1 + T_1$) through a triplet-pair intermediate (TT).[30–34] Both in thin-film studies and dimer-based intramolecular work, the initial formation of TT and its subsequent dissociation into $T_1 + T_1$ or recombination to the ground state are chiefly modeled with single-exponential kinetics.[8,18] This approach signifies that a system's rates of TT formation/recombination/dissociation can be pinpointed to single, unique values. Accordingly, reports of new SF materials describe the rate constant of TT formation or separation that it exhibits. In dimer studies, this framework has highlighted important mechanistic trends: with noteworthy exceptions,[35] a molecule showing fast TT formation also exhibits fast TT recombination.[18] However, moving beyond general dynamical trends to map the rate constants onto specific couplings—an important step for detailed structural design rules—has proved challenging, as highlighted in highly rigid norbornyl-linked dimers.[36] There is growing awareness of the limitations of the standard static framework in non-rigid systems, which can exhibit multiple important conformations. For instance, a limited set of dimers containing diphenylisobenzofuran,[37] tetracene, or pentacene[38] have been reported to exist in two conformations—an SF-active and SF-inactive structure—with structural conversion acting as a switch for SF. A pentacene dimer connected through a flexible crown ether linker revealed solvent-controlled formation of two distinct sub-ensembles in the ground state (weakly coupled monomer-like vs. strongly coupled aggregate), with corresponding TT formation rates that differed by a factor of 250.[39] Similar biexponential TT formation dynamics were reported in π-stacked pentacene dimers encapsulated by polyaromatic capsules, interpreted as an effect of different stacking conformations.[40] Furthermore, a few reports have hinted at the presence of multiple sub-ensembles in conformationally flexible molecular dimers induced by nearly free rotation around acetylene bonds between chromophores. In particular, by controlling the viscosity of the environment through polymer matrices or temperature, it has been revealed that there are significant changes in TT formation and decay dynamics as different sub-ensembles are excited.[41–43] Given this increasing evidence of heterogeneity in the ground/excited states and structural dynamics between different conformers, an important question moving forward is how to properly capture its impact on the dynamics and products of the SF pathway. Nevertheless, the overall kinetics have still been understood on the basis of a static point of view of conformational heterogeneity, with its dynamic aspect rarely invoked.

In this study, we revisit the SF dynamics of a triisopropylsilylethynyl-substituted pentacene (P-TIPS) dimer bridged via acetylene linkers at the 6,6′ position with a phenyldiketopyrrolopyrrole (PDPP), **2P-PDPP** (Figure 1A). We previously reported efficient and fast intramolecular SF in this dimer enabled by synthetic control of the spin density localization and by tuning the electronic nature of the bridge.[44] Here, we focus instead on the role of the acetylene linkers in enabling nearly unimpeded rotation about its axis, which induces conformational heterogeneity with various dihedral

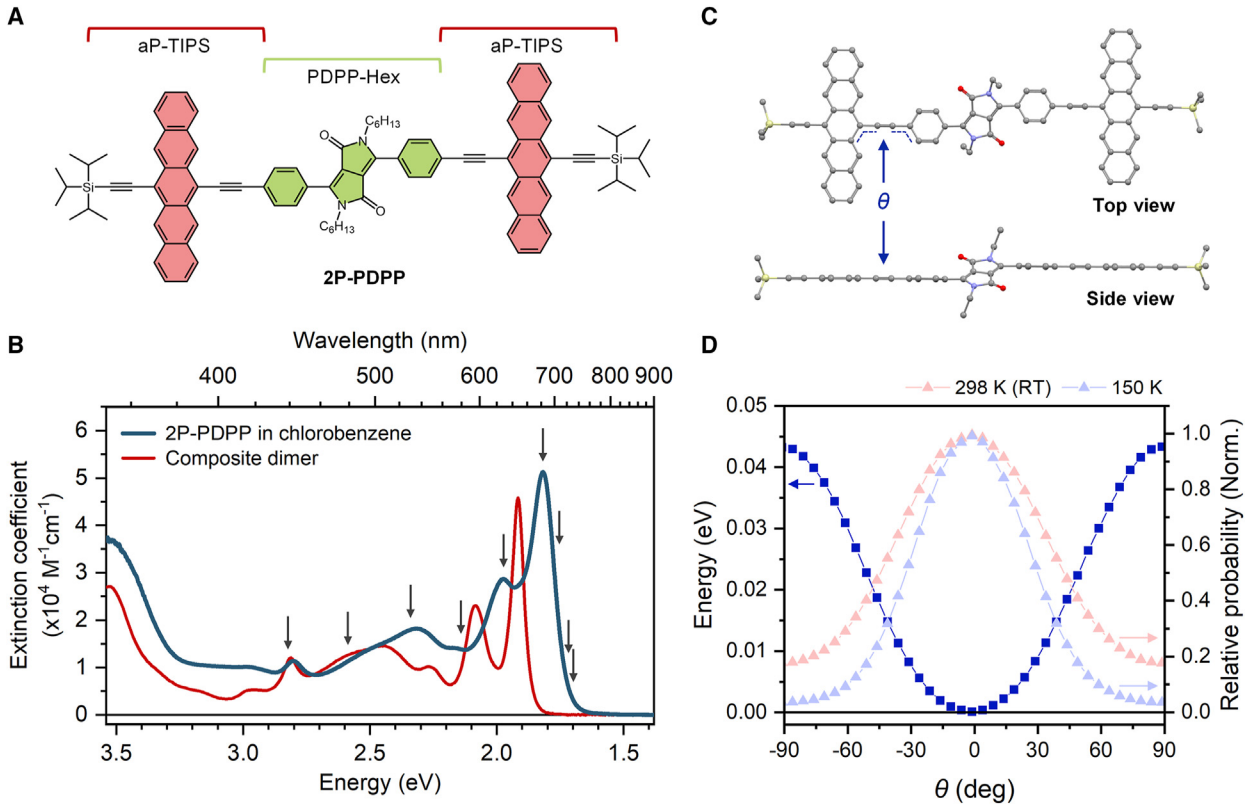

Figure 1. Conformational heterogeneity in the ground state

(A) Chemical structure of **2P-PDPP** composed of two aP-TIPS units linked by a PDPP-Hex chromophore.

(B) Molar extinction coefficient spectrum of **2P-PDPP** in chlorobenzene (solid blue line). The solid red line is a composite spectrum assuming the absence of electronic interactions between aP-TIPS and PDPP-Hex units. The arrows denote excitation energies used in the TA experiments.

(C) The energy-minimized structure of **2P-PDPP** (CAM-B3LYP/6-31g(d) level) in the ground state. Hydrogens are omitted for clarity.

(D) Calculated energy curve (square) in the ground state of **2P-PDPP** along the torsional coordinate θ (i.e., the dihedral angle between phenyl and pentacene planes). Normalized Boltzmann distributions (triangle) in two different temperatures (light red, 298 K; light blue, 150 K) are also shown.

angles among the two P-TIPS units and the PDPP bridge.[41–43] This gives rise to different strengths of inter-pentacene electronic coupling and thereby affects the rate constants for the SF dynamics. Through systematic excitation-energy-dependent transient absorption (TA) experiments at room temperature, we demonstrate that intramolecular ^{1}(TT) formation and recombination cannot simply be defined with monoexponential kinetics and can be markedly more complex than what is reported in many systems to date. We suggest a dynamic picture of intramolecular SF, based on multiple sub-ensembles in the ground state and conversion between these in the excited state. We find that the full range of SF dynamics, spanning from "ultrafast" (<200 fs) to "slow" (<10 ps) TT formation and including multiple TT recombination channels, are controlled by photoexcitation of specific sub-ensembles with different excitation energy. Strikingly, we find that these excitation-energy effects persist out to microsecond spin-evolution processes, resulting in unprecedented selectivity in the spin-polarization patterns of ^{5}(TT) states observed in transient electron paramagnetic resonance (trEPR) spectroscopy. Our findings present a cautionary note that the perspective of both static and dynamic conformational heterogeneity is necessary to describe the photophysics of even simple molecular dimers. Although it poses challenges, embracing this approach offers the scope for ever-deeper insight into the structure-property relationships behind SF and provides a unique avenue to steer the outcome of photophysical processes.

RESULTS AND DISCUSSION

Basic photophysics and molecular structure

As we previously reported, **2P-PDPP** is composed of two aP-TIPS chromophores (here, "a" denotes asymmetric because it has only one TIPS substituent, unlike P-TIPS; Figure S1), which are linked by a PDPP-Hex bridge through acetylene units attached at the 6 or 6′ position of each pentacene.[44] We observe a clear mismatch between the steady-state absorption spectrum of **2P-PDPP** in chlorobenzene and a composite spectrum that assumes non-interacting constituents (Figures 1B and S1). Most importantly, the signature vibronic bands of the parent pentacenes are all considerably red shifted and broadened. The former we attribute to strong electronic interactions between aP-TIPS units via the PDPP-Hex linker, despite their very long center-to-center distance of 23 Å. Indeed, this red shift is markedly more prominent than in other pentacene dimers, for example, the 2,2′- or 6,6′-directly-linked dimers,[14,16] despite their much shorter center-to-center distances. This result highlights the impact of using fully conjugated linkers. Additionally, the absorption band of PDPP-Hex shifts to longer wavelengths from its original position. This serves as further evidence of substantial electronic interaction between the bridging unit and the pentacene moiety. As for the broadening effect, contrary to the Lorentzian-like line shape of bare P-TIPS, **2P-PDPP** instead follows an inhomogeneously broadened Gaussian-like line shape with significantly increased bandwidth. We attribute this effect to conformational heterogeneity due to the shallow torsional potential-energy curve along the rotation axis of the acetylene units, as confirmed by density functional theory (DFT) calculations (Figure 1D). The relatively unimpeded rotation of this bond results in a broad distribution of conformers with different dihedral angles between the two aP-TIPS units and the PDPP-Hex bridge even at 150 K and, consequently, varying degrees of conjugation and electronic coupling strength.[42] The introduction of asymmetric substitution to a pentacene chromophore may enhance its charge transfer characteristics, leading to a broader absorption line shape.[45] However, this effect is less significant than the broadening caused by conformational heterogeneity, which is induced by the rotation of acetylene bonds.[42]

Heterogeneous SF

Figure 2A shows TA spectra of **2P-PDPP** in chlorobenzene after photoexcitation at 1.97 eV corresponding to the 0–1 vibronic absorption. We probed the transient response from 3.44 to 0.75 eV, covering a wide range from ultraviolet (UV) and visible to near-infrared (NIR) regions (see the section "experimental procedures" for experimental details). Right after photoexcitation (0.3 ps), positive bands around 1.9 eV closely match the ground-state absorption to the S_1 state and can be assigned to ground-state bleaching (GSB). A distinct negative photoinduced absorption (PIA) band at 0.93 eV is captured in the NIR, and several further PIA bands are revealed in the UV and visible region (3.44–2.20 eV). Interestingly, through the course of the spectral evolution up to 5 ps, we observe five isosbestic points offset from the baseline (black arrows in Figure 2A). These are a clear marker of population transfer dynamics between two different excited states. Based on our previous work and other reports dealing with the excited-state dynamics of pentacene dimers,[14–16,35,36,39,43,44,46–48] the observed spectral evolution can be ascribed to ^{1}(TT) formation from the initially populated S_1 state. Furthermore, we note that, even at the earliest time delay beyond our instrument response (300 fs), we can already distinguish the characteristic spectral signatures of ^{1}(TT), namely vibronic PIA bands near 2.48 eV and an additional band around 3.2 eV.[14–16,39] The rapid formation of so much ^{1}(TT) population suggests the possibility of an ultrafast, coherent triplet-pair formation channel in **2P-PDPP** despite the very long pentacene center-to-center

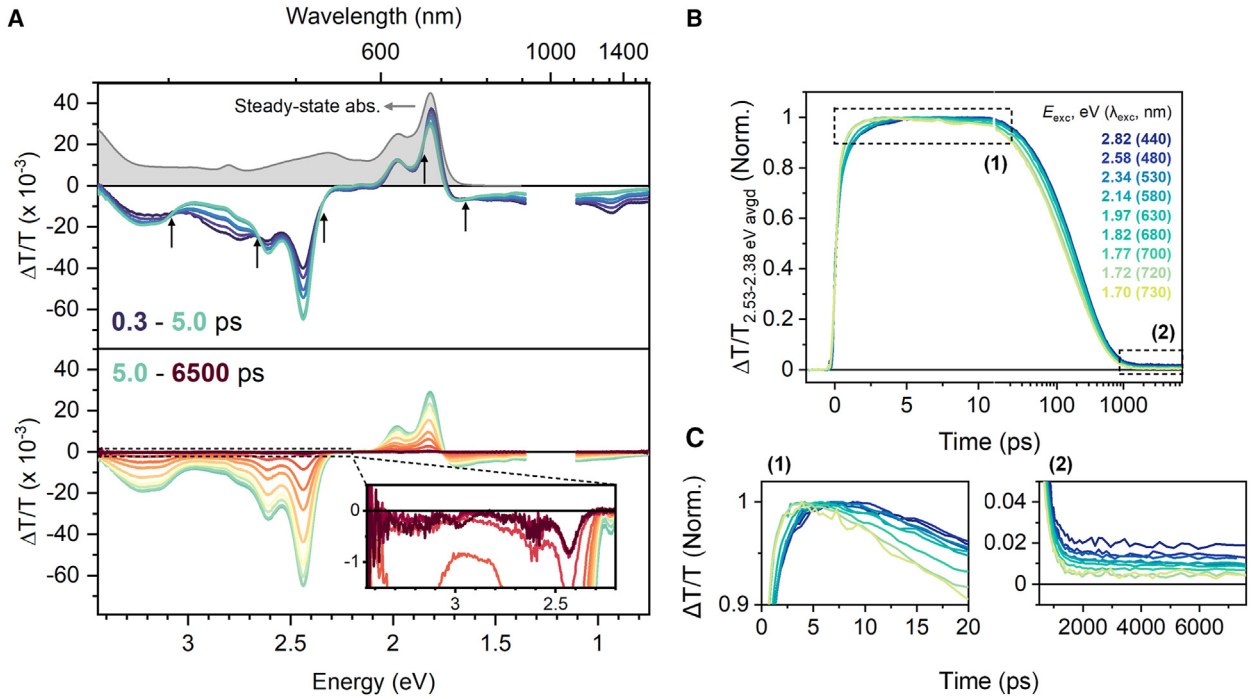

Figure 2. Excitation-energy-dependent ^{1}(TT) formation and recombination

(A) TA spectra of **2P-PDPP** in chlorobenzene at short (0.3–5.0 ps, top) and long (5.0–6,500 ps, bottom) delay times after photoexcitation at 1.97 eV (53.1 μJ/cm^2). The steady-state absorption spectrum (gray shaded) is shown in the upper panel to show the contribution of GSB. The black arrows in the upper panel indicate isosbestic points offset from the baseline, implying direct population transfer from the S_1 to the ^{1}(TT) states. The inset in the lower panel highlights the existence of the long-lived PIA signals after 2 ns.

(B) Excitation-energy-dependent normalized ΔT/T kinetics in ^{1}(TT) absorption region (averaged from 2.53 to 2.38 eV).

(C) The lower panels present enlarged views of the early-time (0–20 ps) and long-time (500–7,600 ps) kinetics.

distance (23 Å; Figure 1C). We return to this topic below. Beyond 5 ps, the principal transient signals from ^{1}(TT) decay uniformly up to 2 ns, leaving a small residual population that does not decay within the detection limit of our delay stage (Figure 2A, inset). Furthermore, we emphasize the uniformity of spectral features and their principal evolution across all excitation energies. Given our excitation sweeps across the characteristic absorption bands of aP-TIPS and PDPP-Hex moieties, this behavior allows us to rule out the possibility of energy or electron transfer from PDPP-Hex to aP-TIPS upon high-energy excitation (Figures S2; S3). Instead, we find that **2P-PDPP** should be treated as a strongly coupled system, in which the units behave as a single quantum entity.

To investigate the possible contribution of conformational heterogeneity, we performed the same measurements for the full range of excitation energies indicated in Figure 1B. In all cases, we observe qualitatively similar TA spectral evolution (Figures S2 and S3), but the corresponding kinetics are systematically modulated. Figure 2B shows normalized ΔT/T kinetics of the main ^{1}(TT) absorption band (averaged over 2.53–2.38 eV). As excitation energy is reduced, both the formation and recombination of ^{1}(TT) accelerate, and the intensity of the long-lived component decreases (Figure 2C).

Focusing first on the early-time dynamics in Figure 2C (left), we note that this timescale matches the typical dynamics of intramolecular vibrational redistribution and vibrational cooling.[49,50] However, these processes carry well-defined signatures, such as progressive shifts of the TA bands,[51] which are absent in our data. Other

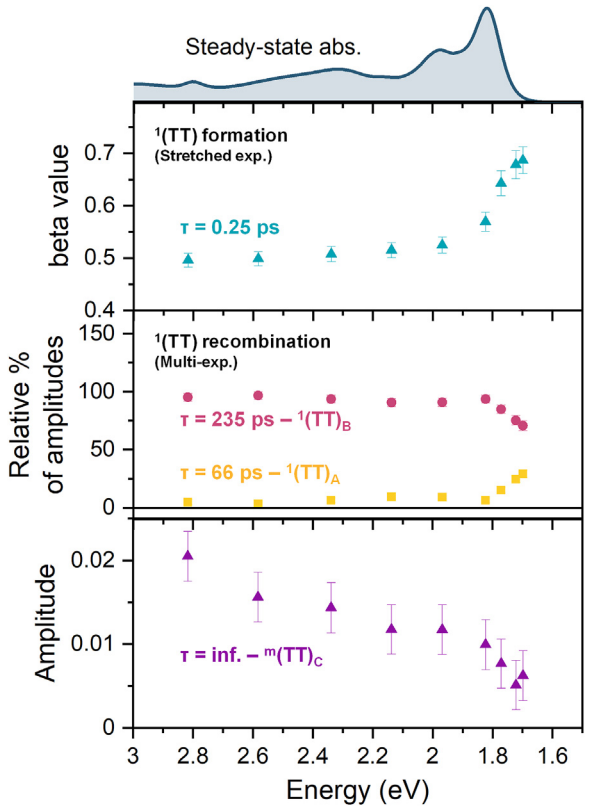

Figure 3. Global fitting results for ^{1}(TT) formation and recombination

Fit lines and residuals are shown in supplemental information. Stretching exponent values, β, depending on excitation energies in ^{1}(TT) formation (top) and relative amplitudes of each component in the multiexponential fitting in ^{1}(TT) recombination (bottom). A, B, and C represent distinct sub-ensembles within the TT states, each characterized by varying degrees of inter-pentacene coupling. This coupling is determined by the dihedral angle between pentacene chromophores and a linker (see Figure 7). The error bars indicate standard errors extracted from the fitting procedures.

reports of excitation-energy-dependent SF dynamics have invoked a model of optically activated branching between two decay pathways from the bright S_1 state, with a new channel (SF) accessible under excess-energy conditions.[23,52] Here, there is no evidence of different types of electronic state accessed with increasing pump energy, and, indeed, the fastest decay rate is obtained following the lowest-energy excitation. We can thus confidently exclude these standard mechanisms for excitation-dependent dynamics (see supplemental information for further details).

Instead, we find that these effects are a direct manifestation of the structural heterogeneity in 2P-PDPP, and we resolve different contributions to this heterogeneity through global kinetic fitting of the excitation-energy dependence, with the key results plotted in Figure 3. Specifically, we found the most satisfactory description of the ^{1}(TT) formation dynamics with a stretched exponential function, while the ^{1}(TT) recombination dynamics could only be globally described with a multiexponential function. We refer the interested reader to the supplemental information for a detailed justification of these two different fitting methods and an alternative approach considering an explicit distribution of lifetimes (Figures S6–S10). For the ^{1}(TT) formation, we determined a global time constant of 250 fs, and the differences between excitation energies can be entirely explained through systematic tuning of

the stretching exponent β from 0.5 at higher pump energies to 0.7 at the red edge (Figure 3). In this type of fit, a β value closer to 1 points to a more uniform (nearly monoexponential) distribution, while values nearing 0 indicate a wider distribution of decay times, suggesting a more heterogeneous system.[53] This demonstrates a broad distribution of ^{1}(TT) formation rates, consistent with the wide range of **2P-PDPP** geometries—and thus pentacene-pentacene coupling strengths—that exist at room temperature. Red-edge excitation narrows this distribution due to the selective excitation of energetically stable conformers, but the fact that β still does not reach 1 highlights the continuing impact of heterogeneity.

In contrast to the continuous distribution of formation rates, the ^{1}(TT) recombination dynamics indicate the system partitions into three distinct time constants—two fast channels of 66 and 235 ps and one long-lived pathway (>8 ns). Indeed, despite the initial geometric disorder upon photoexcitation, the sub-nanosecond decay dynamics cannot be globally described with a similar stretched exponential (Figure S7). It is tempting to map these distinct channels onto a simple sequential pathway of ^{1}(TT) → ^{1}(T … T) (weakly coupled) → T + T, as commonly applied to multi-stage ^{1}(TT) recombination dynamics.[54] However, such a single-ensemble picture cannot explain the systematic excitation-wavelength dependence, especially since the effects persist well beyond the timescale of vibrational relaxation dynamics. Given the inherent structural heterogeneity of **2P-PDPP**, we instead assign the faster decay channels as indicative of different sub-ensembles of ^{1}(TT) states. We denote these as $^1(TT)_A$ and $^1(TT)_B$ (Figure 3) and correlate their different rates of decay to the ground state with different equilibrium geometries. We interpret the appearance of distinct sub-ensembles following the broad distribution of ^{1}(TT) formation rates as a sign of steeper nuclear potentials on the ^{1}(TT) surface than on S_0: within the timescale of tens of picoseconds, the disordered system relaxes toward one of two/three well-defined geometries.

The primary decay amplitude is described by the two fast channels, and the qualitative features of these sub-ensembles can be deduced from their wavelength-dependent amplitudes. The fastest component $^1(TT)_A$ (66 ps) is preferentially generated following low-energy excitation, linking it to the more planarized/conjugated conformers absorbing at the band edge. This result is consistent with the typically observed behavior that a more strongly coupled dimer exhibits faster ^{1}(TT) formation and also faster ^{1}(TT) recombination. The ensemble $^1(TT)_B$ time constant of 235 ps becomes more dominant in higher-energy excitation and likely maps onto conformers with weaker inter-pentacene interactions (i.e., twisted structures). The systematic variation in the relative amplitudes of these decay components hints at a dynamic landscape where the population in each sub-ensemble can be influenced by the excitation energy. Interestingly, we observe that, although red-edge excitation predominantly excites the most structurally stable conformers and enhances the contribution of $^1(TT)_A$, the response remains dominated by longer-lived $^1(TT)_B$. However, an equivalent biexponential analysis of the ^{1}(TT) formation dynamics reveals the opposite behavior (Figure S9), with the dynamics after red-edge excitation dominated by an ultrafast $^1(TT)_A$ channel, with only minor contributions from slower $^1(TT)_B$ formation. The marked change in balance between fast and slow channels in ^{1}(TT) formation and decay reveals an unexpected interconversion from strongly interacting planar $^1(TT)_A$ to weakly interacting twisted $^1(TT)_B$ conformers, even under the lowest-energy excitation. This observation points to an activation barrier between the $^1(TT)_A$ and $^1(TT)_B$ excited-state geometries that can be largely overcome at room temperature and highlights the dynamic perspective of conformational heterogeneity in the excited state.

While $^{1}(TT)_{A}$ and $^{1}(TT)_{B}$ account for the bulk of the population decay, we clearly resolve an additional sub-ensemble denoted $^{m}(TT)_{C}$ (here, we use spin multiplicity "*m*" for this long-lived state instead of 1, due to spin evolution on longer timescales; see below). This species is distinct in that it boasts an average geometry with minimized inter-pentacene coupling. This unique configuration results in such a long lifetime as to permit spin evolution through quintet to free triplets, as laid out below using trEPR. The contribution of sub-ensemble $^{m}(TT)_{C}$ becomes progressively more significant with increasing excitation energy, but it does not follow the same dependence as $^{1}(TT)_{B}$. Our collected observations lead to the intriguing implication that excess excitation energy, before its dissipation to the solvent environment, can steer the system between various $^{1}(TT)$ sub-ensembles and gate the formation of long-lived triplet pairs. Although the similarity in spectral shapes of all TT sub-ensembles makes it challenging to extract dynamics of population transfer between them, we propose this is a stochastic process occurring in competition with vibrational energy transfer and $^{1}(TT)$ recombination timescales.

To further explore the effects of dynamic and static heterogeneity, we conducted control TA experiments on a thin film of **2P-PDPP** embedded in a polystyrene (PS) matrix, where dynamic heterogeneity is inherently minimized.[42,47] Similar to observations in a chlorobenzene solution, the formation and recombination of $^{1}(TT)$ exhibit a clear dependence on pump energy. Intriguingly, however, the kinetics of $^{1}(TT)$ recombination in the PS film necessitates a different model: a biexponential function adequately describes the $^{1}(TT)$ recombination dynamics in the chlorobenzene solution, whereas a tetraexponential function is required for the PS film (Figure S11). This distinction suggests that static heterogeneity plays a more significant role in the dynamics within a rigid medium, while the presence of dynamic heterogeneity in a less viscous medium may reduce the number of distinct sub-ensembles.

Evidence of conformational disorder

We further substantiate our model of heterogeneous SF by analysis of the excitation-energy-dependent TA spectra at early delay time (300 fs). Figures 4A and 4B show normalized TA spectra in the GSB and PIA regions. In general, GSB reflects the ground-state absorption spectrum of the photoexcited molecules, and its shape and peak positions should be in line with the steady-state absorption, although often it can be distorted by overlapping PIA bands. For **2P-PDPP**, we see a good match following excess-energy excitation. On the other hand, as the excitation energy is reduced, the GSB 0-0 band peaks are systematically red shifted. This effect is in accord with our analysis of the dynamics above, where lower-energy excitation preferentially picks out conformers with stronger inter-pentacene interactions. To illustrate this behavior, we use TD-DFT to simulate the optical transitions in three representative conformers out of the continuum of accessible structures: P–P, O–P, and O–O, where P and O denote a co-planar or orthogonal arrangement between pentacene and diketopyrrolopyrrole planes (Figures 4C and 4D). This dihedral angle has a pronounced effect on electronic coupling within the dimer,[41–43] and, accordingly, we observe systematic shifts in the vertical absorption energies between conformers (Figure 4C). The P–P configuration, where both pentacenes align co-planar to the linker plane and delocalization onto the linker should be maximized, exhibits the most red-shifted transition, and we infer that this geometry is predominant during red-edge excitation. Any deviation from this structure causes the transition to blue shift, so we conclude that changing the excitation energy selects different structural distributions with reduced inter-pentacene interactions, resulting in corresponding effects on the GSB spectral shape (Figure 4A). In parallel to these bleaching effects, we observe systematic shifts in the PIA bands in the NIR region

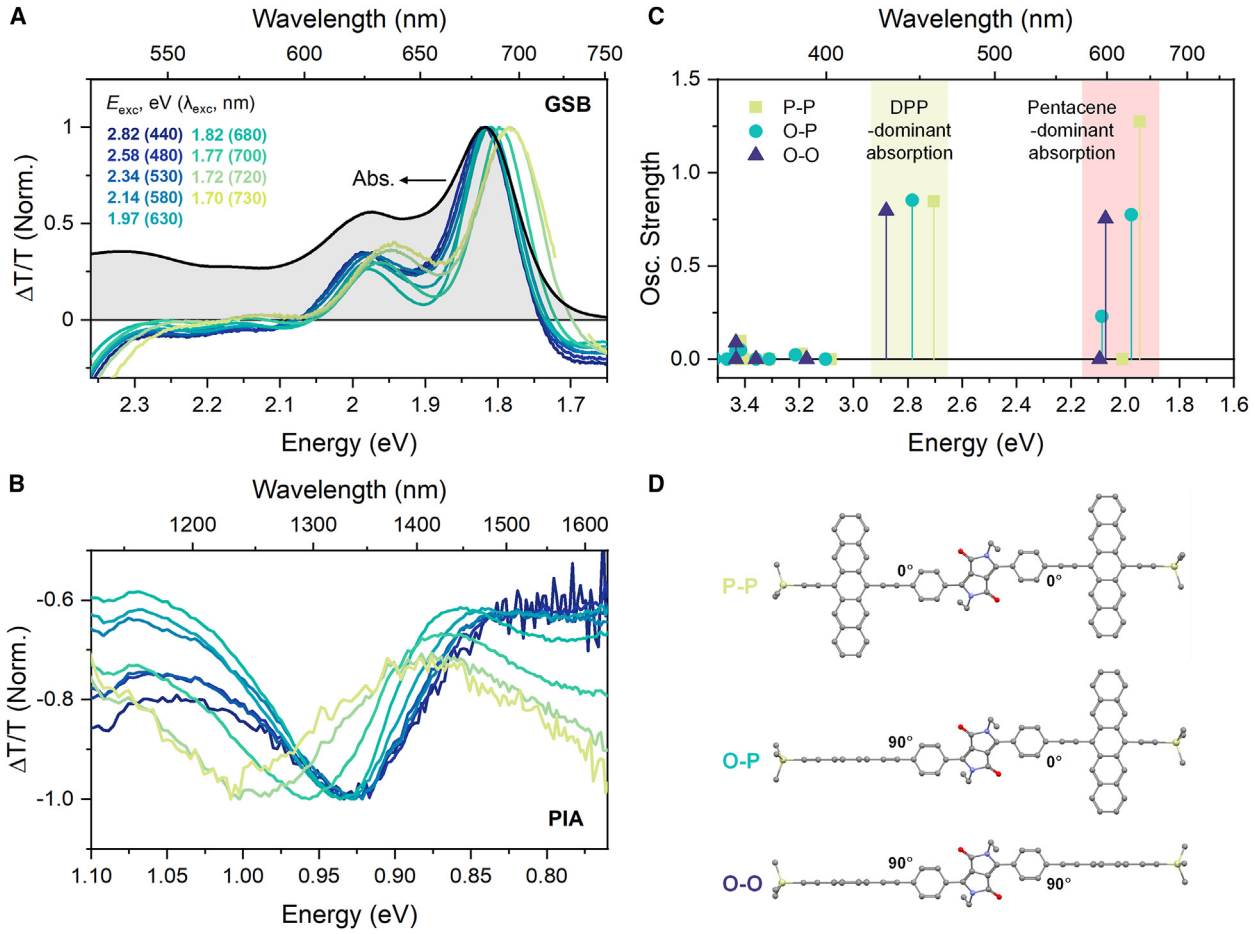

Figure 4. Conformational heterogeneity in the excited state

(A and B) Excitation-energy dependence of normalized ΔT/T spectra at around 300 fs in (A) GSB and (B) PIA regions. Steady-state absorption spectrum (black solid line) is also shown for comparison in (A).

(C) Simulated vertical absorption transitions by TD-DFT method (at CAM-B3LYP/6-31g(d) level of theory) for three representative structures, P–P, O–P, and O–O, of **2P-PDPP**. Each structure is shown in (D). Hydrogens are omitted for clarity and dihedral angles between a phenyl ring and the neighboring pentacene plane are shown for reference.

(Figure 4B). The main S_1 PIA band is located at around 0.925 eV following high-energy excitation, whereas it reveals a blue shift to 1 eV and an increase in the intensity in the vicinity of 0.8 eV upon lowering the excitation energy. This trend is consistent with the gradual variation of the electronic structure along the torsional coordinate in **2P-PDPP**, leading to stabilized S_1 states in more planar conformers. These effects demonstrate that the inhomogeneous broadening highlighted above reflects a range of rotational conformers with different electronic structure defined by torsional disorder.

Ultrafast triplet-pair formation

The type of conformer excited has pronounced effects even on the earliest timescales detected. As noted above, **2P-PDPP** reveals ^{1}(TT) absorption bands at 300-fs delay time, implying an ultrafast SF channel to produce an appreciable ^{1}(TT) population within our ~200-fs instrument response. Because of this initial mixed population, we cannot robustly deconvolve these initial dynamics using standard methods such as global target analysis. Instead, we recall the multiple isosbestic points in the TA spectra detected on longer timescales (Figure 2). Their presence

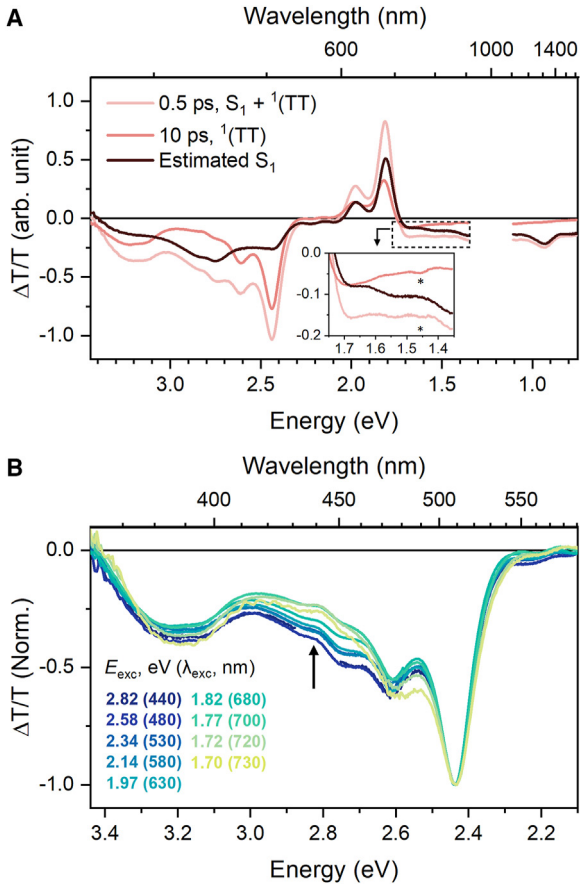

Figure 5. Ultrafast ^{1}(TT) formation controlled by excitation energies

(A) Estimation of the pure S_1 TA spectrum by subtracting the 10-ps spectrum from the 0.5-ps spectrum. The 0.5-ps spectrum is first normalized to the PIA maximum. The 10-ps spectrum is scaled until the characteristic ^{1}(TT) absorption signatures in the estimated S_1 spectrum are minimized. As an example, the inset highlights the ^{1}(TT) PIA band at around 1.46 eV (asterisk), which is totally absent in the estimated pure S_1 spectrum. Spectral decomposition was performed using TA data following 1.97 eV excitation.

(B) Excitation-energy dependence of normalized PIA line shape at 0.5-ps time delay, showing that the contribution of S_1 in the early-time TA spectra becomes smaller as the excitation energy decreases (black arrow).

indicates that SF in **2P-PDPP** can be regarded as a nonadiabatic population transfer from S_1 to ^{1}(TT), rather than an adiabatic evolution along a single surface from S_1-like to ^{1}(TT)-like character. We thus extract the buried TA signature of pure S_1 using decomposition of two TA spectra: the 0.5-ps spectrum, containing information on a mixture of S_1 and ^{1}(TT), and the spectrum at 10 ps, where SF is complete and only ^{1}(TT) is present. As shown in Figure 5A, the estimated S_1 spectrum shows the main PIA at about 2.8 eV, and the overall shape (peak positions and their ratios) closely matches the S_1 signatures in other pentacene dimers and P-TIPS (Figure S14).[36,42,46] This analysis permits the identification of another distinctive excitation-energy effect. Examining the 0.5-ps TA spectra at each excitation energy in Figure 5B, we observe a reduction in the relative weight of the S_1 PIA in the region 2.6–3.3 eV as the excitation energy is reduced (black arrow). That is, we observe progressively less S_1 population remaining on the earliest resolvable timescales. Thus, we conclude that excitation of more planar conformers shifts the balance between S_1 and ^{1}(TT) toward ^{1}(TT) even on ultrafast timescales. We also find that the ultrafast

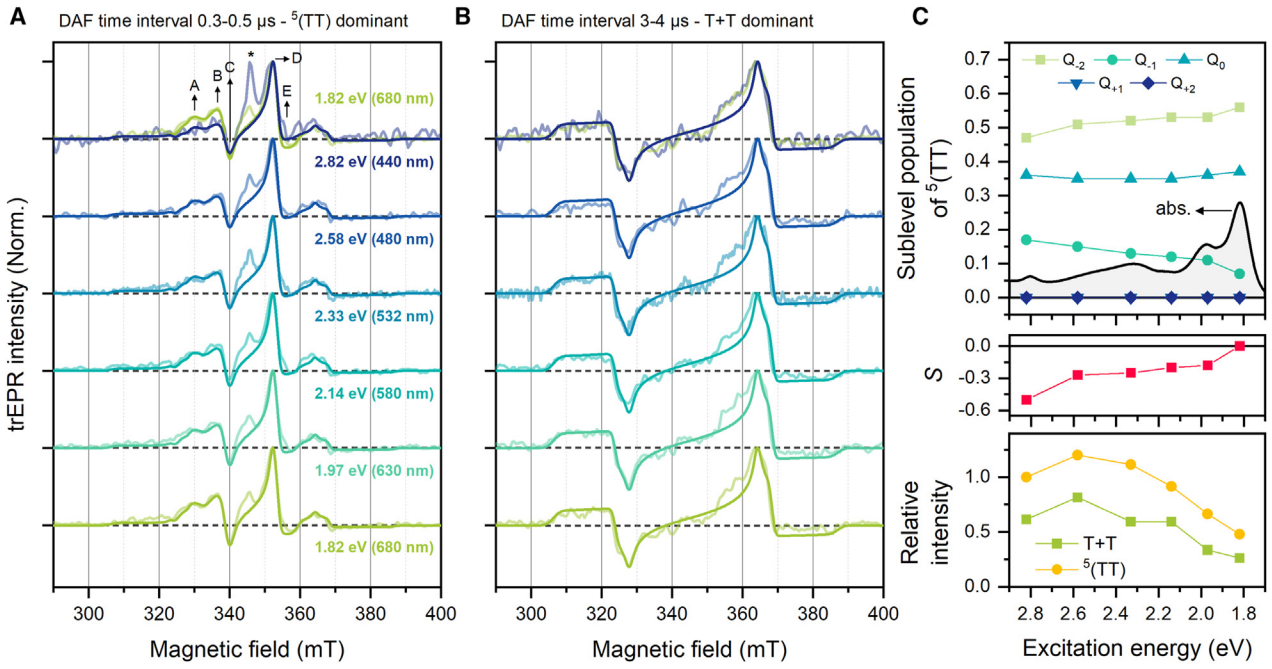

Figure 6. Excitation-energy dependence of long-lived quintet and free triplets

(A and B) trEPR spectra of **2P-PDPP** at (A) early (0.3–0.5 μs) and (B) late (3–4 μs) DAF time intervals after excitation at different excitation energies. (A) and (B) show the contribution of ^{5}(TT), and free triplets (T + T) formed via TT dissociation, respectively. The asterisk in (A) indicates the g = 2 radical signal. The results with the pump energy of 1.82 eV were overlayed on top of those with a 2.82-eV pump to compare the two extreme cases.

(C) Relative sublevel population of ^{5}(TT) (top), orientational ordering parameter S (middle), and relative intensities of ^{5}(TT) and T + T (bottom), depending on excitation energies. The steady-state absorption spectrum in the top panel is also shown for reference.

channel in **2P-PDPP** can lead to approximately 30% ^{1}(TT) yield within 300 fs (Figure S15). The detailed mechanism of this ultrafast process is beyond the scope of the current work and is under further investigation.[55]

The nature of the long-lived spin states

In order to establish the fate of the long-lived $^{m}(TT)_C$ population, we performed trEPR spectroscopy on a frozen 100 μM solution in a 1:1 toluene:*ortho*-dichlorobenzene solvent mixture, which has comparable dielectric properties to chlorobenzene used in the TA, at 150 K. We measure trEPR spectra at a range of excitation energies from 1.82 to 2.82 eV and find that, at early delay-after-flash (DAF) time intervals (0.3–0.5 μs), the spectra are dominated with features corresponding to the quintet state ^{5}(TT) (Figure 6A; transitions shown by labels A–E). The presence of ^{5}(TT) categorically proves SF to be active at all excitation energies.

The quintet spectrum formed after excitation at all measured excitation energies shows the electron spin polarization (ESP) pattern of *aae*/*aea* (where *a* is enhanced absorption and *e* is emission) and can be simulated using the MATLAB toolbox EasySpin with zero-field splitting parameters (ZFS) D_Q = 376.7 MHz, $|E_Q|$ = 12.7 MHz and an exchange coupling (J) of 15 GHz.[56,57] Comparison of the spectral intensities at magnetic field positions 329.5 mT and 336.1 mT (positions A and B in Figure 6A), associated with the $Q_{-2} \rightarrow Q_{-1}$ and shoulder (canonical Z orientation) of $Q_0 \leftrightarrow Q_{\pm 1}$ transition, to the most absorptive quintet peak at 352.3 mT (position D) show important systematic differences. We observe no variation in the quintet dynamics (Figure S24), hence the spectral differences must reflect changes in the nature of the population (see the "trEPR" section in supplemental information for

further discussion). Simulations show that these differences in the spectral shape can be modeled with a decreasing Q_{-2} and simultaneously increasing Q_{-1} relative sublevel population as the excitation energy increases (see Figures 6A and 6C). At 0-0 band excitation (1.82 eV), the relative sublevel populations are [0.56, 0.07, 0.37, 0, 0] going from Q_{-2} to Q_{+2}, while, at high-energy excitation (2.82 eV), the relative populations needed to simulate the experimental results are [0.47, 0.17, 0.36, 0, 0].

At the same time, we find an increase in the orientational ordering parameter (S), which accounts for the degree of selectivity in the spin polarization with the orientation of the molecular axes relative to the external magnetic field. We see that an increasingly negative S is needed to simulate the experimental data when using higher excitation energies ($S_{1.82\ eV} = 0$, $S_{1.97\ eV} = -0.18$, $S_{2.14\ eV} = -0.2$, $S_{2.33\ eV} = -0.25$, $S_{2.58\ eV} = -0.27$, $S_{2.82\ eV} = -0.5$). The increasingly negative S results in decreased intensity at positions B and E compared to D and C. Further discussion related to the orientational ordering parameter are presented in the "trEPR" section in supplemental information. We expect such orientation selectivity to arise due to dipolar contributions to spin mixing between the ^{1}(TT) and ^{5}(TT) manifolds.

It is important to note that, while there are significant changes to the quintet spectrum as a function of excitation energy, the resonance position of the different transitions within the quintet manifold do not change. The separation between the most intense absorptive (position D) and emissive (position C) peaks of the $Q_0 \leftrightarrow Q_{\pm1}$ transition is given by $|D_Q|$-$3|E_Q|$ and when the two chromophores involved in SF are co-planar $|D_Q|$-$3|E_Q| = 1/3(|D_T|$-$3|E_T|)$, where D and E correspond to the quintet and triplet ZFS parameters. We find that the separation between the most absorptive and emissive peaks of the $Q_0 \leftrightarrow Q_{\pm1}$ transitions in our spectra matches the 1/3 relationship with the free triplet ZFS parameters. Hence, in the dimer molecules forming long-lived states, the two aP-TIPS moieties must be in an approximately co-planar configuration. Any deviation from this co-planarity would lead to a decreased quintet spectral width.

Along with the changing quintet spectrum, we also observe an increase in the $g = 2$ signal centered at 346.5 mT (Figure 6A, position marked with an asterisk), which appears as a purely absorptive feature and is largest at the highest excitation energy of 2.82 eV. This absorptive feature increases slightly going from excitation at 1.82—2.58 eV and considerably more when excitation is at 2.82 eV. The ground-state absorption band near 2.82 eV is known to have significant intramolecular charge transfer (CT) character.[24,58] While we do not resolve enough structure to unequivocally attribute the $g = 2$ signal to a CT state, its narrow line shape and the nature of the 2.82 eV excitation band together suggest this is the most likely origin. Further investigation is warranted to establish the origin and its role in the SF process.

The quintet and $g = 2$ signal both show decay on a similar timescale whereby, at a DAF time interval of 3–4 μs, both features disappear (Figure 6B). At these later times, we observe a broader trEPR signal with an ESP pattern of *aee*/*aae* corresponding to the SF-born free triplet ($T_1 + T_1$).[25,59,60] Unlike the quintet, the ESP of the free triplet signal shows no important differences at the various excitation energies, suggesting the mechanism behind the spectral differences only significantly affects the coupled TT pair state and is lost when coherence between the triplets in the pair state dephases. The free triplet spectrum can be simulated using $D_T = 1{,}130$ MHz, $|E_T| = 38$ MHz and a relative sublevel population of [0.25, 0.75, 0.00] from T_{-1} to T_{+1}. The asymmetry in the free triplet signal arises from the greater population of the T_{-1} relative to T_{+1} sublevels, which in part is due to the significant Q_{-2} population,

as population in Q_{-2} results in 2 × T_{-1}[25]. Similarly to the quintet dynamics, the triplet dynamics do not have any excitation-energy dependence (Figure S24). We note that there is additional absorptive signal around 355 mT, which is not accounted for by the triplet simulation in Figure 6B, for all excitation energies. This likely corresponds to remaining quintet signatures with an inverted spin polarization compared to the early-time spectra in Figure 6A.

Finally, we consider the relative intensities of the most absorptive peak for the quintet and free triplet signals, both in the magnetic field and in time, as a function of excitation energy. Taking into account both the excitation fluence and extinction coefficients, we see that the trEPR intensity for quintets and free triplets rises when going from 1.82 to 2.58 eV before slightly decreasing again by 2.82 eV (Figure 6C). While trEPR is not quantitative, a relative comparison is reasonable and consistent with the TA results showing larger yields of long-lived states with higher state excitation (Figure 3). Interestingly, in our solution-phase TA experiments the excitation-energy dependence is linked to dynamic conformational interconversion, but this is not possible in our trEPR experiment. We measure a frozen solution sample where we do not expect large-scale conformational dynamics but only vibrations and small-scale torsional motion. We link the dependence on excitation energy instead to the static distribution of conformers (Figure 1D) and changing character of the initial state. Long-time spin evolution is favored in less coupled conformations and when the excitation targets the higher excited states. The differences in frozen-state trEPR with excitation energy suggests that further mechanistic detail could be obtained by routinely investigating conformational heterogeneity in dimer samples.

Generality of heterogeneous SF

Our systematic excitation-energy-dependent TA and trEPR results for **2P-PDPP** highlight that measurement with a single excitation wavelength is inadequate to fully characterize the SF behavior, nor can a single ensemble with well-defined rate constants describe our observations. The TT formation and recombination dynamics, involvement of a broad conformational distribution and multiple intermediates, and the nature and balance of long-lived states all hinge on an interplay between static and dynamic heterogeneity. Only by evaluating the response of distinct, selectively excited rotational conformers can we capture a unified picture of the complex potential-energy landscapes that govern SF in **2P-PDPP** (Figure 7). While we describe this behavior specifically in the context of **2P-PDPP**, we expect the underlying principles behind conformational heterogeneity and its impact on interchromophore coupling are general. Thus, this behavior likely applies widely to intramolecular SF systems, and we consider that this dynamic picture of heterogeneous SF should supplant the more generally applied static model.

A key criterion for this structural heterogeneity to have an impact is a sufficiently fast rate of SF. In typical systems, vibrational relaxation/cooling or solvation within S_1 will drive most conformers to the same equilibrium geometry. These processes typically occur on approximately picosecond timescales, in exceptional cases into the tens of picoseconds regime,[23] setting a critical threshold for the onset of conformational effects. In tetracene dimers, TT formation is frequently endothermic or isoergic, and it accordingly proceeds over approximately nanosecond timescales where heterogeneity would be unanticipated. On the other hand, a small set of tetracene dimers with strong through-bond coupling reveal much faster TT formation,[41,61] in direct competition with typical vibrational dynamics. In these, we would expect heterogeneous SF to play out through a complex interplay between energetics and S_1-TT couplings, although this was not probed in prior reports. At another extreme, the excess

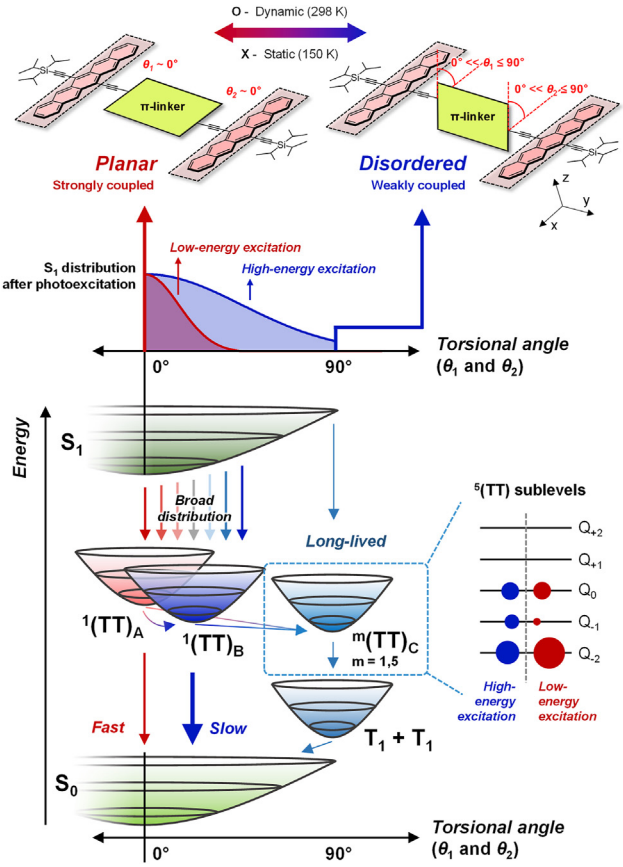

Figure 7. Overview of heterogeneous singlet fission
Schematic illustration of the heterogeneous SF pathways in **2P-PDPP**.

exothermicity of TT formation in hexacene dimers generally results in slow (few-picoseconds timescale) SF,[61], such as electron transfer reactions in the Marcus-inverted region. This timescale is moderately competitive with thermalization, and these materials could likewise reveal heterogeneous SF. The most widely studied SF dimers, though, are composed of pentacenes. With SF energetics ranging from isoergic to moderately exothermic, and widespread reports of sub-ps SF, these model systems are easily the most susceptible to the effects of heterogeneity.

A review of the rich library of reported pentacene dimers suggests that the type of linker and bridging geometry, which controls the interchromophore coupling strength,[18] are likewise determining factors for heterogeneous SF. In the widely studied 2,2′-linked P-TIPS dimer family, phenyl and related bridges can provide some degree of conjugation between pentacenes,[16] but the combination of steric hindrance and the strong local aromaticity of a phenyl ring makes this a relatively minor effect. Hence, the steady-state absorption spectra of most 2,2′ dimers are nearly identical to monomeric pentacenes. They exhibit relatively slow SF, where excess energy in S_1 is dissipated to the surroundings well in advance of TT formation, and we anticipate the excitation energy would have little impact. A key exception is the directly linked (i.e., bridge-free) 2,2′ dimer, where the dihedral angle has been shown to dramatically affect the coupling strength between S_1 and ^{1}(TT).[62] In this system, slight heterogeneity in the inter-pentacene angle should yield significant variation in the initial SF rate. A similar effect is observed in the equivalent

directly linked pentacene dimers with 6,6′ connectivity.[14,47] In polar media, red-edge excitation of these molecules selectively populates a relatively planarized (i.e., more strongly coupled) S_1 state, with the subsequent triplet yield strongly dependent on the relative energy of nearby CT states. Still, in such directly linked dimers, steric hindrance results in steep dihedral angle potentials, meaning that these strongly coupled sub-ensembles are very much a minority population. This limitation is lifted in 6,6′ dimers where the bridge incorporates acetylene linkers,[41,42] a common motif that includes **2P-PDPP**. These moieties simultaneously permit nearly unobstructed dihedral rotation and provide effective conjugation even in torsionally distorted conformations. A hallmark of the enhanced electronic (or vibronic) coupling within the dimers is considerable deviation of their steady-state absorption spectra compared to their monomeric counterparts, as shown in Figure 1. This combination of strong coupling (i.e., rapid SF) and minimal barriers to distortion makes such structures particularly prone to the effects reported here. Indeed, our preliminary measurements on model structures of these dimer families bear this picture out: limited heterogeneity in 2,2′-bipentacene (BP0) versus significant heterogeneity in 6,6′-bipentacene with a *para*-phenyl linker (*p*-2).[15,16] This behavior is currently under further investigation. To meaningfully connect the molecular structure to photophysical function, it is essential to evaluate the behavior of selectively excited sub-ensembles, with especial emphasis on the red-edge excitation to probe the most stable ground-state conformations.

As shown in the foregoing, our combined time-resolved electronic and spin-resonance data for **2P-PDPP** over a range of excitation energies reveals that the choice of conformer affects the timescales of TT formation and recombination, the magnitude of long-lived population, and even the balance of spin sublevels, that is, the full set of important SF characteristics. Interestingly, these ensembles are not static, and the SF kinetics are strongly affected by conformational dynamics (Figure 3). As noted above, we observe that the relative balance of fast channels from $^1(TT)_A$ and slow channels from $^1(TT)_B$ reverses between the TT recombination timescales. This behavior points to structural relaxation within TT that reduces the conjugation and thus the spin-spin exchange coupling that governs the long-time dynamics of TT. Such structural changes are contrary to what is typically observed within S_1 states, where relaxation tends to extend delocalization and increase the interactions between chromophores, but they are consistent with the favorable entropic effects of a distorted TT state.[63,64] Entropy alone provides insufficient driving force, though, since the $^1(TT)_A \rightarrow {}^1(TT)_B$ conversion is suppressed near red-edge excitation. This excitation-energy dependence points to the presence of an activation barrier. We recall that the initial SF dynamics outcompete thermalization within S_1, meaning that the $^1(TT)$ state formed is vibrationally hot. There is thus ample excess energy to drive $^1(TT)_A$ to $^1(TT)_B$ conversion in competition with energy dissipation to the environment, especially following excess-energy excitation. The persistence of this process at reduced efficiency even following red-edge excitation indicates that the relevant torsional barriers are relatively shallow. These barriers reveal an unexpected way that excitation energy can steer relaxation processes within TT and help determine overall triplet yields.

Origin of quintet sublevel population variation

However, it remains challenging within this framework to fully explain the excitation behavior of long-lived $^m(TT)_C$ states. Although the TT formation/recombination effects largely saturate for increasing excitation energies beyond 1.9 eV, the yield of $^1(TT)_C$ monotonically increases through the entire measured range (Figure 3, bottom). The 1 eV energy range spanned dwarfs the torsional barrier (~45 meV) and

is well beyond the range where we would anticipate marked differences in absorption spectra between **2P-PDPP** conformers. Instead, we propose a complementary effect due to the changing character of the initial excitation. In the relevant spectral range, the excitation is increasingly resonant with the PDPP bridge and higher-lying pentacene excited states, both of which are associated with enhanced CT character. Given that we observe no signatures of the PDPP triplet in either trEPR or TA, this behavior could conceivably point to the same kind of sensitization of pentacene SF reported in other acetylene-bridged complexes,[65,66] in our case originating from PDPP singlets. However, comparison with the excitation-dependent TA spectra (Figures 4, 5, S2, and S3) reveals no such sequential progression. In no conditions do we observe a distinct PDPP-centered excitation that transfers to pentacenes, even when the excitation is resonant with the nominal PDPP absorption. Instead, we consider that the entire construct is sufficiently strongly coupled that the chromophore units lose their individual character in the bright state. Within the singlet manifold, it is thus more appropriate to treat **2P-PDPP** as a single electronic unit, similar to previous heterofission constructs.[67] Excitation in different bands may nonetheless shift the character of the mixed electronic state, and we infer that the presence of increased CT character in the initial excitation increases the SF yield in the distorted geometry. While the detailed mechanism of this effect is not clear, it is consistent with the similarly excitation-dependent CT signature observed in trEPR (Figure 6A).

Indeed, the quintet and triplet signals in trEPR, as well as the trends in sublevel populations, follow a strikingly similar energy dependence, indicating that they are governed by a comparable interplay between static and dynamic heterogeneity, including a prominent role for the changing character of higher-energy excited states. We consider it remarkable, though, to observe such similar behavior in such fundamentally different samples. The TA measurements are performed in room-temperature solution, where large-scale conformational dynamics face little barrier. Not only do the frozen solutions used for trEPR drastically limit such conformational change but we obtain quintet signal only for dimers with (near) co-planar pentacenes. In this limited sub-ensemble, through-space pentacene-pentacene coupling is maximized, while the (potentially stronger) through-bond interactions via delocalization across the linker are substantially modulated by the twist of the PDPP-Hex bridge. We expect these conditions are particularly favorable for long-time spin evolution. As we discuss below, the same interplay between static heterogeneity and structural dynamics in this restricted conformational space gives rise to our novel observation of ESP tuning through excitation energy.

Our trEPR study has shown that excitation energies of 1.82 and 2.82 eV lead to distinctive quintet state sublevel populations, and a gradual change between these extremes is observed for intermediate excitation energies (Figure 6C). While the quintet sublevel populations change with excitation energies, the free triplet sublevel populations are rather insensitive. The quintet state spectra of **2P-PDPP** show a decrease in Q_{-2} and increase in Q_{-1} sublevel populations together with an increasingly negative S parameter when utilizing higher excitation energies. To shed some light on the mechanistic differences that give rise to our complex observations, we look to the study by Collins et al., which showed that population of the quintet sublevels is strongly dependent on the time-dependent exchange coupling J.[68] This parameter is considered to change from $|J| \leq |D|$ to $|J| \gg |D|$ during SF and subsequent spin evolution. The change in exchange coupling strength is associated with nuclear reorganization within the molecule(s), and, in the case of dimers, usually torsion of the bridge moiety plays a crucial role. Even at the low temperatures conventionally used for trEPR measurements, this torsional motion is sufficiently active. Collins et al. suggested three parameters that determine the quintet

sublevel populations within the time-dependent exchange coupling model.[68] The first parameter, denoted t_0, is the delay or activation time before the change in exchange coupling and nuclear reorganization occurs. t_0 is non-zero when the excited-state potential surface exhibits an energy barrier to nuclear reorganization. The second parameter is τ_s, which is the statistical lifetime. τ_s governs the distribution in activation times t_0 and gives the probability distribution $P = (1/\tau_s)e^{(-t_0/\tau_s)}$. The last parameter is τ_r, the time taken for the exchange coupling to rise from J_{min} to J_{max} via the relationship $J = J_{max}(1-e^{(-(t-t_0)/\tau_r)})$ for times $t > t_0$. According to this framework, following fast τ_r (e.g., 100 fs), the quintet population will be predominantly in the Q_0 sublevel, while slow τ_r (e.g., 100 ps–10 ns) yields quintet population chiefly in the Q_{-2} and Q_{-1} sublevels. In our case, simulations that do not account for the time-dependent exchange coupling suggest that quintet population is predominantly in the Q_{-2} and Q_0 sublevels.

Quintet sublevel population residing predominately in Q_{-2} and Q_0 is not unusual and was similarly observed for pentacene aggregates in non-glass-forming frozen solution.[69] In this case too, the quintet sublevel population was attributed to a change in the exchange coupling during the SF process, this time from a strongly coupled pair with J_{max} to a weakly coupled pair with J_{min}. The time-dependent exchange coupling was attributed to a change in the TT pair distance occurring due to exciton hopping in a disordered frozen matrix with different aggregate environments. While our trEPR measurements are also in a non-glass-forming frozen solution, we rule out aggregation leading to the observed excitation-dependent quintet spectra based on the excitation-energy-independent quintet and triplet kinetics (Figure S24) and relatively unchanging triplet/quintet ratio (Figure S25). If excitation energy was selecting different aggregate sizes, we would expect differences in the kinetics and the triplet/quintet ratio.[70] Furthermore, a similar quintet spectrum to ours has been observed in a pentacene dimer system in a glass-forming frozen solvent.[46] Hence, we attribute the quintet excitation-energy-dependent spectra to arise from the intramolecular mechanism described by Collins et al. whereby torsional motion results in a time-dependent exchange coupling which, depending on t_0, τ_s, and τ_r, can lead to the observed quintet sublevel populations.[68] It is important to note that, for dimer systems, the change in exchange coupling during SF can be from J_{min} to J_{max} or vice versa, depending on the ground- and excited-state geometries. Here, we identify varying through-bond coupling due to fluctuations in the bridge dihedral angle as the most likely coordinate: this relatively small-scale motion should remain unimpeded even in the frozen matrix.

Tuning of ordering parameters and relative yields of quintet and free triplets

Next, we look to qualitatively explain the increasingly negative S (ordering parameters) needed to model quintet spectra with increasing excitation energies. In the limit of $|J| \leq |D|$, dipolar coupling leads to spin mixing of the $^1(TT)_0$ and $^5(TT)_0$ states to form mixed states, denoted SQ and QS. During the period until t_0 (the activation time for nuclear reorganization) the singlet projection onto the SQ and QS state is time dependent with oscillation periods determined by the ZFS parameters. When the external magnetic field is parallel to the X,Y orientation, the period of oscillation is approximately given by $2\pi/(D_T \pm 3E_T) \sim 5.5$ ns and in the Z orientation by $\pi/D_T \sim 2.78$ ns.[68] At times after t_0, the singlet projection no longer oscillates, and the populations are set by the projections onto SQ and QS. Due to the different oscillation periods at X,Y orientations compared to Z orientations, this leads to different probabilities of $^5(TT)_0$ populations at the different molecular orientations. Therefore, the reason for the observed increasingly negative S with higher excitation energies must be due to t_0 changing such that we move closer to $t_0 = n \times 5.5$ns/2 (where n = 1,3,5 …) and further from $t_0 = m \times 5.5$ ns (m = 1,2,3 …). Since the oscillation period at the X,Y orientation is roughly twice that of the Z orientation, at $n \times 5.5$ns/2 the

maximum intensity of the X,Y orientation would be observed relative to the Z orientation. As t_0 is related to the excited-state potential surface, we propose that higher-energy excitations lead to higher vibrationally excited manifolds resulting in different t_0 values.

Lastly, we come to the increased relative yields of quintet and free triplets with higher excitation energies. While we observe quintet states only from dimers with co-planar pentacenes, as shown by the DFT results even at 150 K a large range of dihedral angles between aP-TIPS and PDPP-Hex can still be occupied. Hence, we expect that bridge heterogeneity (starting geometry) along with its torsional motion (degree of motion accessible) would lead to a wide variety of excited-state potential surfaces, which would have differing degrees of SF quintet and free triplet yields, based on the time-dependent exchange coupling.

While the above discussion only gives qualitative reasoning for the parameters that would govern the quintet state spectra for **2P-PDPP** as a function of different excitation energies, routinely applying such trEPR studies on dimer systems would allow for better understanding of how these parameters differ based on molecular structure, linkers/linker positions, and solvent dielectrics. One key question is whether static heterogeneity in frozen solutions or the higher excited states surfaces accessed through higher excitation energies play the decisive role. In our case, the linker is itself a chromophore, and hence the behavior of this dimer could indeed be more complex than other dimer systems, highlighting the need for more excitation-energy-dependent studies on SF systems. Further work to quantitatively characterize the time-dependent exchange couplings will form the basis of future study.

In conclusion, our research has unveiled the heterogeneous behavior of intramolecular SF in a covalently linked pentacene dimer. Through detailed excitation-energy-dependent TA and trEPR measurements, our findings underscore the significant influence of both dynamic and static disorder on dimer photophysics. Contrary to prevailing assumptions, dimers such as **2P-PDPP** can indeed be exceptionally dynamic. They traverse and sample an expansive range of conformations and electronic couplings throughout their relaxation process. This insight underscores the importance of comprehensive, excitation-energy-dependent investigations. Outside of highly rigid structures, where heterogeneity can be ruled out through careful molecular design, or weakly coupled systems, where the electronic structure and dynamics are dominated by local effects, relying solely on single-point studies can be misleading. A standout revelation from our study is the role of geometric flexibility and disorder—manifested as chromophore rotation in this context. This factor can be advantageous in fostering the generation of long-lived free triplets, especially in the realm of strongly coupled dimers. Such an understanding prompts a paradigm shift in our approach. It suggests that, by dynamically controlling the geometric flexibility and disorder, while simultaneously minimizing other competitive photophysical relaxation pathways, we could optimize the efficiency of generating TT and T + T states or bias the populations of targeted spin sublevels. We believe this realization will pave the way for research that seeks to harness the full potential of the SF processes in not only dimers but also thin films.

EXPERIMENTAL PROCEDURES

Resource availability

Lead contact

Further information and requests for resources should be directed to and will be fulfilled by the lead contact, Andrew J. Musser (ajm557@cornell.edu).

Materials availability

This study did not generate new unique reagents.

Data and code availability

Original data have been deposited to Mendeley Data: https://doi.org/10.17632/jvxtf5gzgc.1. The datasets for the supplemental information are available from the lead contact upon reasonable request.

Sample preparation and steady-state optical characterization

2P-PDPP was prepared according to the reported method. The steady-state absorption spectra of **2P-PDPP** in chlorobenzene were recorded with a home-built absorption spectrometer based on Avantes miniature spectrometer (Avaspec-Mini-40 96CL). Certified chlorobenzene (B255-500, Fisher Chemical) was used without further purification. A solution of 100 mg/mL PS (average molecular weight [M_W] ~ 192,000, 430102, Sigma-Aldrich) and 1.14 mg/mL **2P-PDPP** (1.14 wt %) in toluene (T290-4, Fisher Chemical) was prepared and drop-casted on a pre-cleaned quartz substrate (Ossila).

DFT calculations

DFT calculations were done with Gaussian 16 program.[71] To reduce the computational costs, *n*-hexyl groups in PDPP-Hex and isopropyl groups in aP-TIPSs were replaced by ethyl and methyl groups, respectively. The geometry optimization and potential-energy curve scan calculations were performed using CAM-B3LYP functional[72] with 6-31g(d) basis set[73] for all atoms.

TA spectroscopy

TA measurements were performed with an automated TA spectrometer (HELIOS, Ultrafast Systems) driven by the Yb:KGW amplifier (PHAROS-SP, Light Conversion) operating at 8 kHz. The OPA and SH module (ORPHEUS and LYRA-SH, Light Conversion) generate a 200-fs narrowband pump pulse. A portion of the fundamental was separated to generate a white-light continuum probe pulse ranging from 450 to 1,600 nm using 1-cm sapphire (visible, 450–915 nm) and YAG (NIR, 1,120–1,630 nm) crystal. For UV probe ranging from 350 to 510 nm, the frequency doubled 515 nm was used. The beam diameters ($1/e^2$ height) for pump and probe pulses at the sample position were 650 and 200 μm, respectively. TA spectra were collected with magic-angle condition between pump and probe and in a shot-to-shot fashion. Pump-probe time delay was set by a mechanical delay stage from −3 to 7,600 ps. A 2-mm path length cuvette (Hellma, HL110-2-40) was used. There was no difference in the results regardless of the pump fluence (Figure S9A) and the sample preparation method (ambient vs. inert; Figure S9B).[53,74–76] A magnetic stirrer (Ultrafast Systems) was used to prevent photodegradation of the sample. After every experiment, the steady-state absorption was carefully checked, and we confirmed that there was no degradation of the sample.

trEPR spectroscopy

trEPR experiments were performed on a laboratory-built X-band (9.7 GHz) continuous-wave spectrometer together with a Bruker MD5 dielectric ring resonator with optical access. Optical excitation at 2.33 eV (532 nm) was provided by using a diode-pumped Nd:YAG laser (Atum Laser Titan AC compact 15 MM) equipped with a second harmonic generator, with an incident pulse energy of ~0.525 mJ, a pulse length of 5 ns, and operating at 100-Hz repetition rate. Optical excitation at all other wavelengths was provided by using an Opta OPO (model 355 I, 410–700 nm) pumped by a Spectra-Physics QuantaRay LabSeries 150 Nd:YAG laser

with a pulse length of 7 ns, operating at 10 Hz. The incident pulse energies used for each wavelength are as follows: ~2.24 mJ (1.82 eV, 680 nm), ~3.16 mJ (1.97 eV, 630 nm), ~3.62 mJ (2.14 eV, 580 nm), ~2.02 mJ (2.58 eV, 480 nm), and ~1.02 mJ (2.82 eV, 440 nm). Excitation at each wavelength also included a depolarizer (DPP25-A, Thorlabs) to avoid polarization effects. The temperature was controlled using a Lakeshore 332 temperature controller and a laboratory-built helium flow cryostat. Transients were recorded as the static magnetic field was swept and continuous-wave microwave irradiation was applied (samples were measured with a microwave power of 0.5 mW). The 100 μM sample for trEPR studies was prepared in a nitrogen glovebox in a 1:1 ratio of *ortho*-dichlorobenzene (oDCB) and toluene. Anhydrous toluene and oDCB were purchased from Sigma-Aldrich. The **2P-PDPP** solution was then transferred to a quartz EPR tube with 4-mm outer diameter and attached to a custom adaptor that keeps the solution in the inert nitrogen glovebox atmosphere. The EPR sample was transferred to a pumping station where it underwent several freeze-pump-thaw cycles, before being flame sealed under a vacuum pressure of $\sim 4 \times 10^{-4}$ mbar. EPR simulation was performed using the MATLAB toolbox EasySpin development version 6.0.0-dev.51.[56,57]

SUPPLEMENTAL INFORMATION

Supplemental information can be found online at https://doi.org/10.1016/j.xcrp.2024.102045.

ACKNOWLEDGMENTS

A.J.M. acknowledges the Cornell University College of Arts and Sciences New Frontiers Grant. W.K. is supported by the National Research Foundation of Korea Grant (RS-2023-00210400), funded by the Korean Government. S.P. is supported by Science and Engineering Research Board (SERB), India, through the IRHPA grant (IPA/2020/000033) and core research grant (CRG/2022/004523). N.A.P. and R.B. acknowledge the Deutsche Forschungsgemeinschaft (DFG, German Research Foundation) under Germany's Excellence Strategy (EXC 2008—390540038—UniSysCat). J.D. is supported by The Department of Atomic Energy (DAE), Government of India (12-R&D-TFR-5.10-0100). The DFT calculations were supported by the National Institute of Supercomputing and Network (NISN)/Korea Institute of Science and Technology Information (KISTI) with needed supercomputing resources, including technical support (KSC-2023-CRE-0419). The authors thank Boregowda Puttaraju for useful discussions and Palas Roy (IIT Bhubaneswar) for preliminary transient measurements at TIFR.

AUTHOR CONTRIBUTIONS

Conceptualization, A.J.M. and S.P.; methodology, W.K., N.A.P., K.C.K., and K.M.; investigation, W.K., N.A.P., and A.J.M.; visualization, W.K., N.A.P., and A.J.M.; writing – original draft, W.K., N.A.P., and A.J.M.; writing – review & editing, W.K., N.A.P., K.C.K., K.M., J.D., R.B., S.P., and A.J.M.; supervision, S.P. and A.J.M.

DECLARATION OF INTERESTS

The authors declare no competing interests.

Received: March 16, 2024
Revised: April 10, 2024
Accepted: May 17, 2024
Published: June 11, 2024

REFERENCES

1. Köhler, A., and Bässler, H. (2015). Electronic Processes in Organic Semiconductors (Wiley). https://doi.org/10.1002/9783527685172.

2. Ostroverkhova, O. (2016). Organic Optoelectronic Materials: Mechanisms and Applications. Chem. Rev. *116*, 13279–13412. https://doi.org/10.1021/acs.chemrev.6b00127.

3. Bialas, D., Kirchner, E., Röhr, M.I.S., and Würthner, F. (2021). Perspectives in Dye Chemistry: A Rational Approach toward Functional Materials by Understanding the Aggregate State. J. Am. Chem. Soc. *143*, 4500–4518. https://doi.org/10.1021/jacs.0c13245.

4. Banerji, N., Cowan, S., Vauthey, E., and Heeger, A.J. (2011). Ultrafast Relaxation of the Poly(3-hexylthiophene) Emission Spectrum. J. Phys. Chem. C *115*, 9726–9739. https://doi.org/10.1021/jp1119348.

5. Gélinas, S., Rao, A., Kumar, A., Smith, S.L., Chin, A.W., Clark, J., van der Poll, T.S., Bazan, G.C., and Friend, R.H. (2014). Ultrafast Long-Range Charge Separation in Organic Semiconductor Photovoltaic Diodes. Science *343*, 512–516. https://doi.org/10.1126/science.1246249.

6. Jakowetz, A.C., Böhm, M.L., Sadhanala, A., Huettner, S., Rao, A., and Friend, R.H. (2017). Visualizing excitations at buried heterojunctions in organic semiconductor blends. Nat. Mater. *16*, 551–557. https://doi.org/10.1038/nmat4865.

7. Wilson, M.W.B., Rao, A., Clark, J., Kumar, R.S.S., Brida, D., Cerullo, G., and Friend, R.H. (2011). Ultrafast Dynamics of Exciton Fission in Polycrystalline Pentacene. J. Am. Chem. Soc. *133*, 11830–11833. https://doi.org/10.1021/ja201688h.

8. Yost, S.R., Lee, J., Wilson, M.W.B., Wu, T., McMahon, D.P., Parkhurst, R.R., Thompson, N.J., Congreve, D.N., Rao, A., Johnson, K., et al. (2014). A transferable model for singlet-fission kinetics. Nat. Chem. *6*, 492–497. https://doi.org/10.1038/nchem.1945.

9. Johnson, J.C., Nozik, A.J., and Michl, J. (2013). The Role of Chromophore Coupling in Singlet Fission. Acc. Chem. Res. *46*, 1290–1299. https://doi.org/10.1021/ar300193r.

10. Carrod, A.J., Gray, V., and Börjesson, K. (2022). Recent advances in triplet–triplet annihilation upconversion and singlet fission, towards solar energy applications. Energy Environ. Sci. *15*, 4982–5016. https://doi.org/10.1039/D2EE01600A.

11. Stern, H.L., Cheminal, A., Yost, S.R., Broch, K., Bayliss, S.L., Chen, K., Tabachnyk, M., Thorley, K., Greenham, N., Hodgkiss, J.M., et al. (2017). Vibronically coherent ultrafast triplet-pair formation and subsequent thermally activated dissociation control efficient endothermic singlet fission. Nat. Chem. *9*, 1205–1212. https://doi.org/10.1038/nchem.2856.

12. Pensack, R.D., Tilley, A.J., Parkin, S.R., Lee, T.S., Payne, M.M., Gao, D., Jahnke, A.A., Oblinsky, D.G., Li, P.-F., Anthony, J.E., et al. (2015). Exciton Delocalization Drives Rapid Singlet Fission in Nanoparticles of Acene Derivatives. J. Am. Chem. Soc. *137*, 6790–6803. https://doi.org/10.1021/ja512668r.

13. Finton, D.M., Wolf, E.A., Zoutenbier, V.S., Ward, K.A., and Biaggio, I. (2019). Routes to singlet exciton fission in rubrene crystals and amorphous films. AIP Adv. *9*, 095027. https://doi.org/10.1063/1.5118942.

14. Lukman, S., Musser, A.J., Chen, K., Athanasopoulos, S., Yong, C.K., Zeng, Z., Ye, Q., Chi, C., Hodgkiss, J.M., Wu, J., et al. (2015). Tuneable Singlet Exciton Fission and Triplet–Triplet Annihilation in an Orthogonal Pentacene Dimer. Adv. Funct. Mater. *25*, 5452–5461. https://doi.org/10.1002/adfm.201501537.

15. Zirzlmeier, J., Lehnherr, D., Coto, P.B., Chernick, E.T., Casillas, R., Basel, B.S., Thoss, M., Tykwinski, R.R., and Guldi, D.M. (2015). Singlet fission in pentacene dimers. Proc. Natl. Acad. Sci. USA *112*, 5325–5330. https://doi.org/10.1073/pnas.1422436112.

16. Sanders, S.N., Kumarasamy, E., Pun, A.B., Trinh, M.T., Choi, B., Xia, J., Taffet, E.J., Low, J.Z., Miller, J.R., Roy, X., et al. (2015). Quantitative Intramolecular Singlet Fission in Bipentacenes. J. Am. Chem. Soc. *137*, 8965–8972. https://doi.org/10.1021/jacs.5b04986.

17. Hetzer, C., Guldi, D.M., and Tykwinski, R.R. (2018). Pentacene Dimers as a Critical Tool for the Investigation of Intramolecular Singlet Fission. Chem. Eur J. *24*, 8245–8257. https://doi.org/10.1002/chem.201705355.

18. Korovina, N.V., Pompetti, N.F., and Johnson, J.C. (2020). Lessons from intramolecular singlet fission with covalently bound chromophores. J. Chem. Phys. *152*, 040904. https://doi.org/10.1063/1.5135307.

19. Young, R.M., and Wasielewski, M.R. (2020). Mixed Electronic States in Molecular Dimers: Connecting Singlet Fission, Excimer Formation, and Symmetry-Breaking Charge Transfer. Acc. Chem. Res. *53*, 1957–1968. https://doi.org/10.1021/acs.accounts.0c00397.

20. Hong, Y., Schlosser, F., Kim, W., Würthner, F., and Kim, D. (2022). Ultrafast Symmetry-Breaking Charge Separation in a Perylene Bisimide Dimer Enabled by Vibronic Coupling and Breakdown of Adiabaticity. J. Am. Chem. Soc. *144*, 15539–15548. https://doi.org/10.1021/jacs.2c03916.

21. Hong, Y., Kim, W., Kim, T., Kaufmann, C., Kim, H., Würthner, F., and Kim, D. (2022). Real-time Observation of Structural Dynamics Triggering Excimer Formation in a Perylene Bisimide Folda-dimer by Ultrafast Time-Domain Raman Spectroscopy. Angew. Chem. Int. Ed. *61*, e202114474. https://doi.org/10.1002/anie.202114474.

22. Schnedermann, C., Alvertis, A.M., Wende, T., Lukman, S., Feng, J., Schröder, F.A.Y.N., Turban, D.H.P., Wu, J., Hine, N.D.M., Greenham, N.C., et al. (2019). A molecular movie of ultrafast singlet fission. Nat. Commun. *10*, 4207. https://doi.org/10.1038/s41467-019-12220-7.

23. Alvertis, A.M., Lukman, S., Hele, T.J.H., Fuemmeler, E.G., Feng, J., Wu, J., Greenham, N.C., Chin, A.W., and Musser, A.J. (2019). Switching between Coherent and Incoherent Singlet Fission via Solvent-Induced Symmetry Breaking. J. Am. Chem. Soc. *141*, 17558–17570. https://doi.org/10.1021/jacs.9b05561.

24. Parenti, K.R., Chesler, R., He, G., Bhattacharyya, P., Xiao, B., Huang, H., Malinowski, D., Zhang, J., Yin, X., Shukla, A., et al. (2023). Quantum interference effects elucidate triplet-pair formation dynamics in intramolecular singlet-fission molecules. Nat. Chem. *15*, 339–346. https://doi.org/10.1038/s41557-022-01107-8.

25. Tayebjee, M.J.Y., Sanders, S.N., Kumarasamy, E., Campos, L.M., Sfeir, M.Y., and McCamey, D.R. (2017). Quintet multiexciton dynamics in singlet fission. Nat. Phys. *13*, 182–188. https://doi.org/10.1038/nphys3909.

26. Dean, J.C., Zhang, R., Hallani, R.K., Pensack, R.D., Sanders, S.N., Oblinsky, D.G., Parkin, S.R., Campos, L.M., Anthony, J.E., and Scholes, G.D. (2017). Photophysical characterization and time-resolved spectroscopy of a anthradithiophene dimer: exploring the role of conformation in singlet fission. Phys. Chem. Chem. Phys. *19*, 23162–23175. https://doi.org/10.1039/C7CP03774K.

27. Bradley, S.J., Chi, M., White, J.M., Hall, C.R., Goerigk, L., Smith, T.A., and Ghiggino, K.P. (2021). The role of conformational heterogeneity in the excited state dynamics of linked diketopyrrolopyrrole dimers. Phys. Chem. Chem. Phys. *23*, 9357–9364. https://doi.org/10.1039/D1CP00541C.

28. Söderberg, M., Dereka, B., Marrocchi, A., Carlotti, B., and Vauthey, E. (2019). Ground-State Structural Disorder and Excited-State Symmetry Breaking in a Quadrupolar Molecule. J. Phys. Chem. Lett. *10*, 2944–2948. https://doi.org/10.1021/acs.jpclett.9b01024.

29. Qiu, W., Liu, D., Li, M., Cai, X., Chen, Z., He, Y., Liang, B., Peng, X., Qiao, Z., Chen, J., et al. (2023). Confining donor conformation distributions for efficient thermally activated delayed fluorescence with fast spin-flipping. Nat. Commun. *14*, 2564. https://doi.org/10.1038/s41467-023-38197-y.

30. Smith, M.B., and Michl, J. (2010). Singlet Fission. Chem. Rev. *110*, 6891–6936. https://doi.org/10.1021/cr1002613.

31. Miyata, K., Conrad-Burton, F.S., Geyer, F.L., and Zhu, X.-Y. (2019). Triplet Pair States in Singlet Fission. Chem. Rev. *119*, 4261–4292. https://doi.org/10.1021/acs.chemrev.8b00572.

32. Sanders, S.N., Pun, A.B., Parenti, K.R., Kumarasamy, E., Yablon, L.M., Sfeir, M.Y., and Campos, L.M. (2019). Understanding the Bound Triplet-Pair State in Singlet Fission. Chem *5*, 1988–2005. https://doi.org/10.1016/j.chempr.2019.05.012.

33. Musser, A.J., and Clark, J. (2019). Triplet-Pair States in Organic Semiconductors. Annu. Rev. Phys. Chem. *70*, 323–351. https://doi.org/10.1146/annurev-physchem-042018-052435.

34. Kim, W., and Musser, A.J. (2021). Tracking ultrafast reactions in organic materials through vibrational coherence: vibronic coupling mechanisms in singlet fission. Adv. Phys. X *6*, 1918022. https://doi.org/10.1080/23746149.2021.1918022.

35. Kumarasamy, E., Sanders, S.N., Tayebjee, M.J.Y., Asadpoordarvish, A., Hele, T.J.H., Fuemmeler, E.G., Pun, A.B., Yablon, L.M., Low, J.Z., Paley, D.W., et al. (2017). Tuning Singlet Fission in π-Bridge-π Chromophores. J. Am. Chem. Soc. *139*, 12488–12494. https://doi.org/10.1021/jacs.7b05204.

36. Gilligan, A.T., Miller, E.G., Sammakia, T., and Damrauer, N.H. (2019). Using Structurally Well-Defined Norbornyl-Bridged Acene Dimers to Map a Mechanistic Landscape for Correlated Triplet Formation in Singlet Fission. J. Am. Chem. Soc. *141*, 5961–5971. https://doi.org/10.1021/jacs.9b00904.

37. Schrauben, J.N., Akdag, A., Wen, J., Havlas, Z., Ryerson, J.L., Smith, M.B., Michl, J., and Johnson, J.C. (2016). Excitation Localization/Delocalization Isomerism in a Strongly Coupled Covalent Dimer of 1,3-Diphenylisobenzofuran. J. Phys. Chem. A *120*, 3473–3483. https://doi.org/10.1021/acs.jpca.6b00826.

38. Yamakado, T., Takahashi, S., Watanabe, K., Matsumoto, Y., Osuka, A., and Saito, S. (2018). Conformational Planarization versus Singlet Fission: Distinct Excited-State Dynamics of Cyclooctatetraene-Fused Acene Dimers. Angew. Chem. Int. Ed. *57*, 5438–5443. https://doi.org/10.1002/anie.201802185.

39. Aster, A., Zinna, F., Rumble, C., Lacour, J., and Vauthey, E. (2021). Singlet Fission in a Flexible Bichromophore with Structural and Dynamic Control. J. Am. Chem. Soc. *143*, 2361–2371. https://doi.org/10.1021/jacs.0c12384.

40. Catti, L., Narita, H., Tanaka, Y., Sakai, H., Hasobe, T., Tkachenko, N.V., and Yoshizawa, M. (2021). Supramolecular Singlet Fission of Pentacene Dimers within Polyaromatic Capsules. J. Am. Chem. Soc. *143*, 9361–9367. https://doi.org/10.1021/jacs.0c13172.

41. Korovina, N.V., Joy, J., Feng, X., Feltenberger, C., Krylov, A.I., Bradforth, S.E., and Thompson, M.E. (2018). Linker-Dependent Singlet Fission in Tetracene Dimers. J. Am. Chem. Soc. *140*, 10179–10190. https://doi.org/10.1021/jacs.8b04401.

42. Ringström, R., Edhborg, F., Schroeder, Z.W., Chen, L., Ferguson, M.J., Tykwinski, R.R., and Albinsson, B. (2022). Molecular rotational conformation controls the rate of singlet fission and triplet decay in pentacene dimers. Chem. Sci. *13*, 4944–4954. https://doi.org/10.1039/D1SC06285A.

43. Majumder, K., Mukherjee, S., Panjwani, N.A., Lee, J., Bittl, R., Kim, W., Patil, S., and Musser, A.J. (2023). Controlling Intramolecular Singlet Fission Dynamics via Torsional Modulation of Through-Bond versus Through-Space Couplings. J. Am. Chem. Soc. *145*, 20883–20896. https://doi.org/10.1021/jacs.3c06075.

44. Krishnapriya, K.C., Roy, P., Puttaraju, B., Salzner, U., Musser, A.J., Jain, M., Dasgupta, J., and Patil, S. (2019). Spin density encodes intramolecular singlet exciton fission in pentacene dimers. Nat. Commun. *10*, 33. https://doi.org/10.1038/s41467-018-07736-3.

45. Lehnherr, D., McDonald, R., and Tykwinski, R.R. (2008). Exploring Electronically Polarized Pentacenes. Org. Lett. *10*, 4163–4166. https://doi.org/10.1021/ol801464k.

46. Basel, B.S., Zirzlmeier, J., Hetzer, C., Phelan, B.T., Krzyaniak, M.D., Reddy, S.R., Coto, P.B., Horwitz, N.E., Young, R.M., White, F.J., et al. (2017). Unified model for singlet fission within a non-conjugated covalent pentacene dimer. Nat. Commun. *8*, 15171. https://doi.org/10.1038/ncomms15171.

47. Lukman, S., Chen, K., Hodgkiss, J.M., Turban, D.H.P., Hine, N.D.M., Dong, S., Wu, J., Greenham, N.C., and Musser, A.J. (2016). Tuning the role of charge-transfer states in intramolecular singlet exciton fission through side-group engineering. Nat. Commun. *7*, 13622. https://doi.org/10.1038/ncomms13622.

48. Trinh, M.T., Pinkard, A., Pun, A.B., Sanders, S.N., Kumarasamy, E., Sfeir, M.Y., Campos, L.M., Roy, X., and Zhu, X.-Y. (2017). Distinct properties of the triplet pair state from singlet fission. Sci. Adv. *3*, e1700241. https://doi.org/10.1126/sciadv.1700241.

49. Braem, O., Penfold, T.J., Cannizzo, A., and Chergui, M. (2012). A femtosecond fluorescence study of vibrational relaxation and cooling dynamics of UV dyes. Phys. Chem. Chem. Phys. *14*, 3513–3519. https://doi.org/10.1039/c2cp23167k.

50. Horng, M.L., Gardecki, J.A., Papazyan, A., and Maroncelli, M. (1995). Subpicosecond Measurements of Polar Solvation Dynamics: Coumarin 153 Revisited. J. Phys. Chem. *99*, 17311–17337. https://doi.org/10.1021/j100048a004.

51. Basel, B.S., Zirzlmeier, J., Hetzer, C., Reddy, S.R., Phelan, B.T., Krzyaniak, M.D., Volland, M.K., Coto, P.B., Young, R.M., Clark, T., et al. (2018). Evidence for Charge-Transfer Mediation in the Primary Events of Singlet Fission in a Weakly Coupled Pentacene Dimer. Chem *4*, 1092–1111. https://doi.org/10.1016/j.chempr.2018.04.006.

52. Musser, A.J., Al-Hashimi, M., Maiuri, M., Brida, D., Heeney, M., Cerullo, G., Friend, R.H., and Clark, J. (2013). Activated Singlet Exciton Fission in a Semiconducting Polymer. J. Am. Chem. Soc. *135*, 12747–12754. https://doi.org/10.1021/ja405427j.

53. Beckwith, J.S., Rumble, C.A., and Vauthey, E. (2020). Data analysis in transient electronic spectroscopy – an experimentalist's view. Int. Rev. Phys. Chem. *39*, 135–216. https://doi.org/10.1080/0144235X.2020.1757942.

54. Pensack, R.D., Ostroumov, E.E., Tilley, A.J., Mazza, S., Grieco, C., Thorley, K.J., Asbury, J.B., Seferos, D.S., Anthony, J.E., and Scholes, G.D. (2016). Observation of Two Triplet-Pair Intermediates in Singlet Exciton Fission. J. Phys. Chem. Lett. *7*, 2370–2375. https://doi.org/10.1021/acs.jpclett.6b00947.

55. Musser, A., Kim, J., Bain, D., Ding, V., Majumder, K., Windemuller, D., Feng, J., Wu, J., Patil, S., Anthony, J., and Kim, W. (2023). Coherent Photoexcitation of Entangled Triplet Pair States. Res Sq. https://doi.org/10.21203/rs.3.rs-3483408/v1.

56. Stoll, S., and Schweiger, A. (2006). EasySpin, a comprehensive software package for spectral simulation and analysis in EPR. J. Magn. Reson. *178*, 42–55. https://doi.org/10.1016/j.jmr.2005.08.013.

57. Tait, C.E., Krzyaniak, M.D., and Stoll, S. (2023). Computational tools for the simulation and analysis of spin-polarized EPR spectra. J. Magn. Reson. *349*, 107410. https://doi.org/10.1016/j.jmr.2023.107410.

58. Hele, T.J.H., Fuemmeler, E.G., Sanders, S.N., Kumarasamy, E., Sfeir, M.Y., Campos, L.M., and Ananth, N. (2019). Anticipating Acene-Based Chromophore Spectra with Molecular Orbital Arguments. J. Phys. Chem. A *123*, 2527–2536. https://doi.org/10.1021/acs.jpca.8b12222.

59. Weiss, L.R., Bayliss, S.L., Kraffert, F., Thorley, K.J., Anthony, J.E., Bittl, R., Friend, R.H., Rao, A., Greenham, N.C., and Behrends, J. (2017). Strongly exchange-coupled triplet pairs in an organic semiconductor. Nat. Phys. *13*, 176–181. https://doi.org/10.1038/nphys3908.

60. Bayliss, S.L., Weiss, L.R., Kraffert, F., Granger, D.B., Anthony, J.E., Behrends, J., and Bittl, R. (2020). Probing the Wave Function and Dynamics of the Quintet Multiexciton State with Coherent Control in a Singlet Fission Material. Phys. Rev. X *10*, 021070. https://doi.org/10.1103/PhysRevX.10.021070.

61. Sanders, S.N., Kumarasamy, E., Fallon, K.J., Sfeir, M.Y., and Campos, L.M. (2019). Singlet fission in a hexacene dimer: energetics dictate dynamics. Chem. Sci. *11*, 1079–1084. https://doi.org/10.1039/C9SC05066C.

62. Fuemmeler, E.G., Sanders, S.N., Pun, A.B., Kumarasamy, E., Zeng, T., Miyata, K., Steigerwald, M.L., Zhu, X.-Y., Sfeir, M.Y., Campos, L.M., and Ananth, N. (2016). A Direct Mechanism of Ultrafast Intramolecular Singlet Fission in Pentacene Dimers. ACS Cent. Sci. *2*, 316–324. https://doi.org/10.1021/acscentsci.6b00063.

63. Hasobe, T., Nakamura, S., Tkachenko, N.V., and Kobori, Y. (2022). Molecular Design Strategy for High-Yield and Long-Lived Individual Doubled Triplet Excitons through Intramolecular Singlet Fission. ACS Energy Lett. *7*, 390–400. https://doi.org/10.1021/acsenergylett.1c02300.

64. Korovina, N.V., Chang, C.H., and Johnson, J.C. (2020). Spatial separation of triplet excitons drives endothermic singlet fission. Nat. Chem. *12*, 391–398. https://doi.org/10.1038/s41557-020-0422-7.

65. Gotfredsen, H., Thiel, D., Greißel, P.M., Chen, L., Krug, M., Papadopoulos, I., Ferguson, M.J., Nielsen, M.B., Torres, T., Clark, T., et al. (2023). Sensitized Singlet Fission in Rigidly Linked Axial and Peripheral Pentacene-Subphthalocyanine Conjugates. J. Am. Chem. Soc. *145*, 9548–9563. https://doi.org/10.1021/jacs.2c13353.

66. Lavarda, G., Zirzlmeier, J., Gruber, M., Rami, P.R., Tykwinski, R.R., Torres, T., and Guldi, D.M. (2018). Tuning Intramolecular Förster Resonance Energy Transfer and Activating Intramolecular Singlet Fission. Angew. Chem. Int. Ed. *57*, 16291–16295. https://doi.org/10.1002/anie.201808652.

67. Sanders, S.N., Kumarasamy, E., Pun, A.B., Steigerwald, M.L., Sfeir, M.Y., and Campos, L.M. (2016). Intramolecular Singlet Fission in Oligoacene Heterodimers. Angew. Chem. Int. Ed. *55*, 3373–3377. https://doi.org/10.1002/anie.201510632.

68. Collins, M.I., McCamey, D.R., and Tayebjee, M.J.Y. (2019). Fluctuating exchange interactions enable quintet multiexciton formation in singlet fission. J. Chem. Phys. *151*, 164104. https://doi.org/10.1063/1.5115816.

69. Nagashima, H., Kawaoka, S., Akimoto, S., Tachikawa, T., Matsui, Y., Ikeda, H., and Kobori, Y. (2018). Singlet-Fission-Born Quintet State: Sublevel Selections and Trapping by Multiexciton Thermodynamics. J. Phys. Chem. Lett. *9*, 5855–5861. https://doi.org/10.1021/acs.jpclett.8b02396.

70. Orsborne, S.R.E., Gorman, J., Weiss, L.R., Sridhar, A., Panjwani, N.A., Divitini, G., Budden, P., Palecek, D., Ryan, S.T.J., Rao, A., et al. (2023). Photogeneration of Spin Quintet Triplet–Triplet Excitations in DNA-Assembled Pentacene Stacks. J. Am. Chem. Soc. *145*, 5431–5438. https://doi.org/10.1021/jacs.2c13743.

71. Frisch, M.J., Trucks, G.W., Schlegel, H.B., Scuseria, G.E., Robb, M.a., Cheeseman, J.R., Scalmani, G., Barone, V., Petersson, G.a., Nakatsuji, H., et al. (2016). Gaussian 16, Revision C.01 (Gaussian, Inc.).

72. Yanai, T., Tew, D.P., and Handy, N.C. (2004). A new hybrid exchange–correlation functional using the Coulomb-attenuating method (CAM-B3LYP). Chem. Phys. Lett. *393*, 51–57. https://doi.org/10.1016/j.cplett.2004.06.011.

73. Petersson, G.A., Bennett, A., Tensfeldt, T.G., Al-Laham, M.A., Shirley, W.A., and Mantzaris, J. (1988). A complete basis set model chemistry. I. The total energies of closed-shell atoms and hydrides of the first-row elements. J. Chem. Phys. *89*, 2193–2218. https://doi.org/10.1063/1.455064.

74. Chang, M.-H., Hoffmann, M., Anderson, H.L., and Herz, L.M. (2008). Dynamics of Excited-State Conformational Relaxation and Electronic Delocalization in Conjugated Porphyrin Oligomers. J. Am. Chem. Soc. *130*, 10171–10178. https://doi.org/10.1021/ja711222c.

75. Kim, W., Tahara, S., Kuramochi, H., Takeuchi, S., Kim, T., Tahara, T., and Kim, D. (2021). Mode-Specific Vibrational Analysis of Exciton Delocalization and Structural Dynamics in Conjugated Oligomers. Angew. Chem. Int. Ed. *60*, 16999–17008. https://doi.org/10.1002/anie.202102168.

76. Slavov, C., Hartmann, H., and Wachtveitl, J. (2015). Implementation and Evaluation of Data Analysis Strategies for Time-Resolved Optical Spectroscopy. Anal. Chem. *87*, 2328–2336. https://doi.org/10.1021/ac504348h.